The Little Duke Breccia Mineral System: IOCG Geochemical Vectors in the Eastern Succession Cloncurry

Professor Ken Collerson
PhD., FAusIMM

KDC Consulting
ABN 44 584 455 091
Brisbane, Queensland

February 20th 2019

TABLE OF CONTENTS

Certificate of Qualified Person

I, Emeritus Professor Kenneth D. Collerson, am the Principal of KDC Consulting (KDC^2) 33 Cramond St, Wilston, 4051 Queensland, Australia.

This certificate applies to this technical report titled ***The Little Duke Breccia Mineral System: IOCG Geochemical Vectors*** that has an effective date of 20th February, 2019.

I am a Fellow of the Australasian Institute of Mining and Metallurgy (#100125). I graduated in 1993 as Doctor of Philosophy (Geology) from the University of Adelaide, South Australia and also have a Bachelor of Science degree with 1st Class Honours from University of New England, N.S.W., Australia (awarded in 1997). Emeritus Professorial status at the University of Queensland acknowledges of my contribution to research, management and teaching in the University sector.

I have practiced my profession as a Principal Consultant with Salva Resources, HDR Salva and Caracle Creek (Toronto) and as a self-employed consultant for more than 35 years. As a Principal Consultant in mineral exploration I have an excellent record of discovery. I have worked on a variety of multi-commodity metals exploration projects through high-level consulting activities in more than 15 countries.

In a consultancy for Geological Survey of Queensland (2014-2016) using spinifex grass as a biogeochemical exploration medium in the Simpson Desert, in 2014 I discovered a Devonian age alkaline metallogenic province, (Diamantina Province). Importantly, I showed that the Diamantina Province is part of a much larger belt (a plume track) of ~ 440 Ma to 365 Ma igneous activity that extends more than 2000 km from central NSW to the Northern Territory. The entire belt is prospective for a range of metals including scandium, cobalt, PGEs, copper, and gold, as well as for diamond.

Recent industry and government consultancies include:

- Qld., Dept. Natural Resources and Mines December 2018 - Cobalt and HREE Mineral Systems in the Mount Isa Block.
- AusMex Ltd September 2018 -Rare Earth Element - Cobalt-Copper-Gold Mineral System at Burra, S.A: Significance of the AusLAMP Magnetotelluric Anomaly
- Hammer Metals August 2018 - U-Pb Titanite Geochronological Constraints on Origin and Age of the Mount Philip Breccia
- Northern Cobalt June 2018 - Review of Wollogorang Project Chemistry: Mineral System and Exploration Vectors.
- Longford Resources Feb. 2018 - present. Targeting Co and PGE mineralisation in the Goodsprings area, Nevada.
- Hammer Metals Feb. 2018 - present. Identification of key mineralisation geochemical vectors, as well as mineralisation and alteration styles in the Mary Kathleen Belt
- Encounter Resources May 2017 - present. Spinifex biogeochemistry proof of concept survey over gold and Co anomalies in the Telfer area, WA
- Laconia Resources Ltd May 2017 - present. Au-Ni-PGE target generation in the Kraaipan Greenstone Belt, Botswana
- Caracle Creek International 2016 - present. Associate Pegmatite Specialist Providing field geological, petrological and geochemical advice for international clients on exploration for LCT pegmatites

- Tyranna Resources June 2016 - present. Improved understanding of calcrete gold geochemistry in the western Gawler Craton that allowed discrimination between true and false calcrete Au anomalies with great success.
- Macarthur Lithium 2016. Provided field geological, petrological and geochemical advice to the MD on lithium exploration in the Pilbara and Yilgarn Cratons. Developed a technique using trace elements in K-feldspar to identify the Li content of the source pegmatite. This IP has global application.
- Impact Minerals Ltd 2015 - present. Petrology and geochemistry of outcrop and drill core samples from Red Hill and Mulga Springs-Moorkaie Intrusions at Broken Hill. Decoded the geochemistry and petrology of PGE-Au-Cu-Ni-Zn mineralisation at Broken Hill, resulting in enhanced understanding of the entire mineral system at Broken Hill, one of Earth's largest accumulations of metals.
- Providence Natural Resources 2012 - present. LCT pegmatite exploration for lithium at Järkvissle in Central Sweden. Currently contracted to find a JV Partner for a JORC Li resource.
- Exco/Copper Chem 2014. Preparation of a geological briefing paper for the Mary Kathleen rare earth Government tender bid.
- Exco 2014. Preparation of a prospectivity assessment for the White Dam area, South Australia, specifically identifying geochemical vectors that allowed improved understanding of the style of mineralisation.
- Chinalco Yunnan Copper Resources Limited 2013 - April 2014.Reviewed and reinterpreted drill core at Elaine and Blue Caesar and developed new model for Cu-Au-Co-REE-U mineralisation in the Mary Kathleen Belt, NW Queensland. I identified the alkaline igneous source of metals in the terrane and demonstrated that these ~1526 Ma alkaline intrusions were emplaced at a shallow crustal depth and produced epithermal mineralisation. As well as improving knowledge of Mary Kathleen Belt mineral systems, this discovery also explains Cloncurry Belt IOCG mineralisation.
- Viti Mining Pty Ltd. 2013 April - Present. Confirmed the existence of world-class very high-grade Mn mineralisation (DSO) at a number of locations on Viti Levu, Fiji. Showed that mineralisation was hydrothermal and occurred as part of an epithermal alteration system above Au-Ag-Cu bearing shoshonite intrusions
- Golden Island Resources Pty Ltd. 2013 April - Present. Undertook a literature review and discovered "lost" reports showing very widely distributed high grade Au and Ag assays (up to 35 g/t) on Waya and Wayasewa. Showed that these islands formed an extension of the shoshonite – gold trend west of Viti Levu, and following recovery of excellent panned concentrate results the islands are now being investigated using soil geochemistry to delineate drill targets.
- Golden Island Resources Pty Ltd. 2013 April - Present. I reprocessed magnetic and gravity data for Viti Levu and discovered a previously unknown ~40 km diameter Au-bearing shoshonite caldera south of Tavua caldera that has never been drilled. The Tavua caldera is host for the >1MOz epithermal Au-Ag Emperor goldmine on Viti Levu.
- Waratah Resources 2012 December. Prospectivity assessment of Gabon and the Republic of the Congo. Reviewed the geochemistry of BIFs in Waratah Resources tenements in Gabon and the Republic of the Congo to facilitate regional exploration and resource estimation.
- ASERA Iron Project 2012. December Geochemical evaluation of Lake Vättern orthomagmatic Fe-Ti-V project, Southern Sweden. Concluded that mineralisation is hosted by an anorogenic anorthosite intrusion not IOCG as previously believed.
- Triton Gold 2012 – August to December. Geochemical interpretation, Au and Mn target assessment on Viti Levu.
- Pacific Wildcat Resources 2011 – July to October. Fieldwork in Kenya and interpretation of DD core from Mrima Hill carbonatite and outcrops of nepheline

syenite in a nearby intrusion. Showed that carbonatites and syenites were genetically related forming part of a >10 km diameter intrusion. Discovered an untested mineral system and identified zones of rare earth mineralisation for a subsequent RC and DD drilling program.

I am responsible for all sections of this report and am independent of the Department of Natural Resources and Mines as is described by Section 1.5 of NI 43-101.

I am confident that this report has been prepared in compliance with the JORC 2012 Code and with the instrument NI 43-101.

As of the effective date of the technical report, to the best of my knowledge, information and interpretation in the report contains all scientific and technical details that are required to be disclosed.

Dated 20th February , 2019

Professor Kenneth D. Collerson

Ph.D., FAusIMM

1 Executive Summary

Principal conclusions of this review are as follows:

- The Little Duke breccia system is a high-level epithermal system that is proximal to an ultramafic to mafic igneous source of halogen-rich fluids and metals that include Co, Ni, Cu, As, Au, Ag, PGEs.
- Although earlier studies of the IOCG mineral system in the Cloncurry area suggested that Cu, Au, F, U, P and REEs, as well as S were derived from the Williams Naraku Granite via a magmatic-hydrothermal fluid (Williams et al., 2015), given the element association (Co, Ni, PGE's and Au), a more plausible explanation is that metals in the system were derived from an ultramafic to mafic alkaline igneous source.
- High levels of positively correlated Ni, Co and Cu confirm the role of olivine fraction in the igneous source of the Little Duke breccia. This metal association simply cannot be explained by a granitic source.
- Positively correlated S with Ni, Co, Cu and As also confirms the involvement of magmatic/hydrothermal processes below Little Duke.
- Correlations between Te, Bi and Sb with Au, indicates that the breccia system is proximal to the igneous source of the Little Duke mineral system.
- Halogen-rich fluids that form halogen complexes are conducive to fluid - metal transport. These fluids are interpreted to have existed at Little Duke, where dissociation of halogen complexes likely occurred in response to changes of the hydrothermal environment such as fluid–rock interaction, fluid mixing, cooling, and phase separation.
- Molar Cu/Au ratios are controlled initially by magma source chemistries and subsequently by the physical-chemical evolution of the ore forming hydrothermal fluids. Little Duke samples with molar Cu/Au ratios between ~30,000 and 100,000 are typical of alkaline igneous systems.
- La/Yb - HREE systematics also support an ultramafic to mafic igneous source and suggest the possible presence of HREE enriched alteration haloes proximal to the Little Duke breccia system.
- Sub-and super-chondritic Y/Ho ratios indicate the involvement of halogen-rich hydrothermal fluids in the Little Duke breccia system.
- Primitive mantle normalized highly siderophile element abundance (Ni, PGE, Au and Cu) plots exhibit similar levels of enrichment and fractionation patterns to deposits in the Mary Kathleen Belt. This suggests that both Cloncurry belt and the adjacent Mary Kathleen Belt were influenced by the same metal fertile plume magmatic source. Given this similarity, it is considered highly improbable that any of the HSEs were derived from an alkaline granitic source as suggested by Kendrick et al., (2007) and Williams et al., (2015).
- The presence of a log normal Ag/Au distribution reflects precious metal transport in boiling solutions, confirming a high level epithermal depositional environment associated with hot springs (Cole and Drummond, 1986).
- The epithermal deposits along the Golden Mile, from Guilded Rose to Mount Freda are Au rich. Covariation of Au with Bi and Te indicates the close relationship to an igneous source (Marinova et al., 2013).

- The presence of these features indicates that hot springs occurred above IOCG source intrusions in the Cloncurry area and explains the occurrence of high concentrations of Au in the district.
- The presence of a large magnetotelluric conductive anomaly below the Ernest Henry IOCG deposit (Wang et al., 2018) is similar to the MT anomaly below Olympic Dam and likely reflects the lithospheric response of the metal migration regime associated with this plume generated world class IOCG system (Heinson et al., 2018).
- Thus it is likely that the same fluorine-rich and oxidizing hydrothermal fluids that formed the Olympic Dam IOCG deposits remained active as the plume track migrated to the north east and generated the Cloncurry Belt IOCG mineralisation.
- The data indicates that Little Duke is likely to be proximal to a deeper and fertile IOCG mineral system.
- Thus the Little Duke data is highly significant and it is recommended that diamond core drilling should continue in the RC holes to target the deeper source IOCG or ISCG alkaline igneous of the metal anomalism.

2 Introduction

Objectives of this study were: (1) to evaluate and interpret multi-element assay results from recent RC drilling of the Little Duke breccia; (2) to better understand the origin of Mesoproterozoic Cu-Ni-Co-Au-PGE-REE mineral systems in AusMex's tenure south of Cloncurry; (3) to gain insight into possible IOCG (or ISCG) proximal and distal geochemical vectors, and (4) to comment on the metallogenic significance of electrical conductivity structures identified with magnetotelluric data below IOCG deposits in the Cloncurry area.

3Little Duke Prospect

Little Duke is one of a number of prospects on AusMex Ltds. tenements between Guilded Rose and Mount Freda (Figure 1).

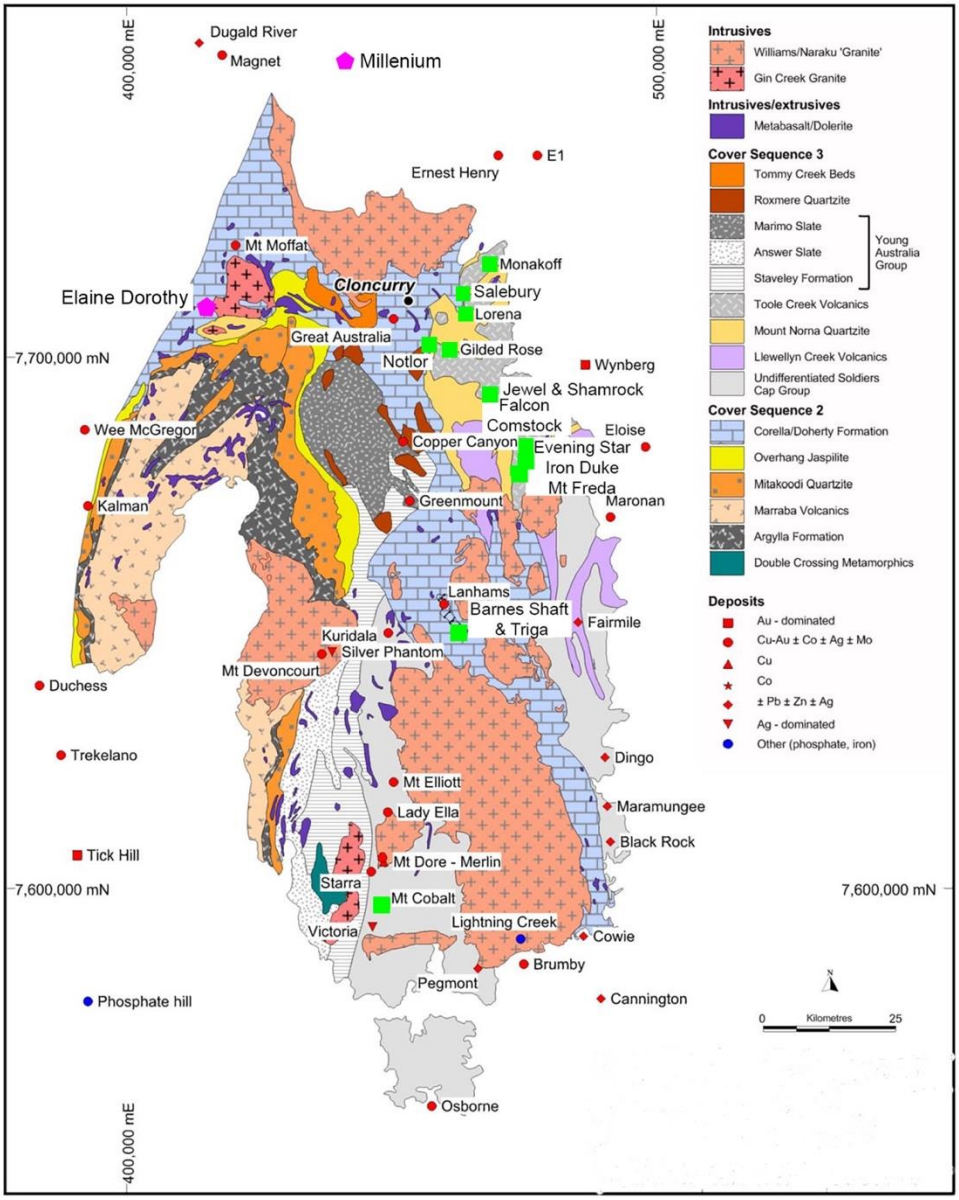

Figure 1: Map showing geology of the eastern Mount Isa Block from Collerson (2018). Locations of deposits in this study are shown by green squares.

4 Geochemistry

4.1 Analytical Techniques

Assay data in this report are from AusMex recently completed RC drilling campaign at Little Duke. Samples are from drill hole LD18RC006 and cover the depth interval from 48 m to 132 m. They were analysed by Australian Laboratory Services Pty Ltd. at Stafford in Brisbane.

Major and trace element data were obtained using the techniques listed in Table 1. Element detection limits are also reported in Table 1.

Table 1: Detection Limits for ALS Analytical Procedures

Element	Units	Det. Limit	Method	Element	Units	Det.Limit	Method
Au	ppm	0.001	PGM-ICP24	Nb	ppm	0.1	ME-MS61
Ag	ppm	0.01	ME-MS61	Nd	ppm	0.1	ME-MS61
Al	%	0.01	ME-MS61	Ni	ppm	0.2	ME-MS61
As	ppm	0.2	ME-MS61	P	ppm	10	ME-MS61
Ba	ppm	10	ME-MS61	Pb	ppm	0.5	ME-MS61
Be	ppm	0.05	ME-MS61	Pd	ppm	0.01	PGM-ICP24
Bi	ppm	0.01	ME-MS61	Pr	ppm	0.03	ME-MS61
Ca	%	0.01	ME-MS61	Pt	ppm	0.005	PGM-ICP24
Cd	ppm	0.02	ME-MS61	Rb	ppm	0.1	ME-MS61
Ce	ppm	0.01	ME-MS61	Re	ppm	0.002	ME-MS61
Co	ppm	0.1	ME-MS61	S	%	0.01	ME-MS61
Cr	ppm	1	ME-MS61	Sb	ppm	0.05	ME-MS61
Cs	ppm	0.05	ME-MS61	Sc	ppm	0.1	ME-MS61
Cu	ppm	0.2	ME-MS61	Se	ppm	1	ME-MS61
Dy	ppm	0.05	ME-MS61	Sm	ppm	0.03	ME-MS61
Er	ppm	0.03	ME-MS61	Sn	ppm	0.2	ME-MS61
Eu	ppm	0.03	ME-MS61	Sr	ppm	0.2	ME-MS61
Fe	%	0.01	ME-MS61	Ta	ppm	0.05	ME-MS61
Ga	ppm	0.05	ME-MS61	Tb	ppm	0.01	ME-MS61
Gd	ppm	0.05	ME-MS61	Te	ppm	0.05	ME-MS61
Ge	ppm	0.05	ME-MS61	Th	ppm	0.01	ME-MS61
Hf	ppm	0.1	ME-MS61	Ti	%	0.005	ME-MS61
Ho	ppm	0.01	ME-MS61	Tl	ppm	0.02	ME-MS61
In	ppm	0.005	ME-MS61	Tm	ppm	0.01	ME-MS61
K	%	0.01	ME-MS61	U	ppm	0.1	ME-MS61
La	ppm	0.5	ME-MS61	V	ppm	1	ME-MS61
Li	ppm	0.2	ME-MS61	W	ppm	0.1	ME-MS61
Lu	ppm	0.01	ME-MS61	Y	ppm	0.1	ME-MS61
Mg	%	0.01	ME-MS61	Yb	ppm	0.03	ME-MS61
Mn	ppm	5	ME-MS61	Zn	ppm	2	ME-MS61
Mo	ppm	0.05	ME-MS61	Zr	ppm	0.5	ME-MS61
Na	%	0.01	ME-MS61				

Table 2: Selected Trace Element Data for Little Duke RC Samples

	Au	Pt	Pd	Ag	Sc	V	Cr	Co	Ni	Cu	Zn
	ppm	ppb	ppb	ppm	ppm	ppm	ppm	ppm	ppm	ppm	ppm
LD18RC006_48_49	0.129		2	0.76	19	609	14	214	82	4630	27
LD18RC006_49_50	0.287		2	1.00	34	879	11	329	138	6260	18
LD18RC006_50_51	0.542		2	1.00	20	178	7	369	146	5450	19
LD18RC006_51_52	2.19		1	1.29	20	131	14	502	191	8640	30
LD18RC006_52_53	2.72		2	1.52	27	88	10	644	206	9420	33
LD18RC006_53_54	3.13		2	1.88	28	71	12	698	213	9290	34
LD18RC006_54_55	2.5		3	1.46	30	115	13	644	193	8200	45
LD18RC006_55_56	1.77		4	0.98	30	131	13	574	154	5430	44
LD18RC006_56_57	0.533		1	0.53	33	22	4	183	75	2880	24
LD18RC006_57_58	0.621		1	0.21	24	97	19	131	51	1320	23
LD18RC006_58_59	0.083		1	0.13	28	294	36	71	47	743	20
LD18RC006_59_60	0.073			0.10	30	316	36	61	47	634	23
LD18RC006_59_60B	0.088		1	0.11	30	288	34	58	47	768	22
LD18RC006_59_60C	0.002			0.01		4	5	3	4	36	<2
LD18RC006_60_61	0.043			0.07	26	272	34	35	38	380	38
LD18RC006_61_62	0.024			0.05	23	248	43	25	34	284	22
LD18RC006_62_63	0.008			0.03	12	156	41	15	20	150	19
LD18RC006_63_64	0.029		1	0.03	14	143	44	113	36	155	20
LD18RC006_64_65	0.076		2	0.03	11	113	42	21	32	124	19
LD18RC006_65_66	0.012		1	0.04	14	112	40	28	33	193	23
LD18RC006_66_67	0.016		1	0.04	12	120	46	30	24	133	38
LD18RC006_67_68	0.016		4	0.03	13	125	41	28	20	125	21
LD18RC006_68_69	0.146	112	160	0.03	12	127	41	21	14	115	17

LD18RC006_69_70	0.038		2	0.22	13	125	43	20	15	1750	22
LD18RC006_70_71	0.03		3	0.06	11	99	39	24	28	254	47
LD18RC006_71_72	0.014			0.04	12	93	39	31	34	193	88
LD18RC006_72_73	0.01			0.04	11	101	39	21	34	86	34
LD18RC006_73_74	0.683		2	0.54	13	87	33	164	54	2990	27
LD18RC006_74_75	1.29		1	1.25	16	25	10	393	76	7060	31
LD18RC006_75_76	0.461		1	0.42	13	39	16	149	40	1520	25
LD18RC006_76_77	1.01		2	0.64	13	59	19	215	46	2970	26
LD18RC006_77_78	4.73			1.17	15	19	7	982	121	6780	37
LD18RC006_78_79	2.67		1	0.96	17	16	5	251	47	4580	44
LD18RC006_79_80	0.475		1	0.42	16	8	2	177	21	2270	22
LD18RC006_79_80B	0.467			0.39	17	8	2	185	21	2290	21
LD18RC006_79_80C	0.016			0.04	1	3	15	9	3	132	3
LD18RC006_80_81	0.327			0.31	18	14	6	323	39	859	18
LD18RC006_81_82	0.712			0.41	20	9	3	464	45	1190	22
LD18RC006_82_83	0.64		2	0.72	15	53	17	419	58	2990	21
LD18RC006_83_84	2.23		3	0.81	13	41	12	366	59	3960	29
LD18RC006_84_85	1.425			0.44	17	13	6	763	72	2500	42
LD18RC006_85_86	0.665		1	0.90	13	12	10	720	71	4920	32
LD18RC006_86_87	1.675		1	0.69	17	6	4	211	40	4160	24
LD18RC006_87_88	0.652		1	1.64	6	10	12	941	104	10200	36
LD18RC006_88_89	1.46			2.17	6	21	10	464	108	13950	36
LD18RC006_89_90	2.03		2	1.12	9	8	6	403	148	6660	34
LD18RC006_90_91	1.315			0.81	14	35	10	362	88	4790	34
LD18RC006_91_92	0.864		2	0.31	30	306	24	62	32	2160	65
LD18RC006_92_93	0.024		1	0.08	40	436	26	43	36	469	50
LD18RC006_93_94	0.201		2	0.49	26	260	24	70	35	2820	31

LD18RC006_94_95	1.34		2	0.80	16	118	18	137	48	4590	48
LD18RC006_95_96	0.499		3	0.36	11	80	18	98	40	2340	24
LD18RC006_96_97	0.438	5		0.37	14	105	25	152	49	2040	50
LD18RC006_97_98	0.184			0.30	11	97	33	85	34	718	25
LD18RC006_98_99	0.075			0.20	8	88	29	45	17	886	27
LD18RC006_99_100	0.951		3	1.11	10	55	18	128	52	5450	36
LD18RC006_99_100B	1.06			1.25	10	49	19	167	55	6020	38
LD18RC006_99_100C	0.032			0.05	1	6	3	9	3	130	12
LD18RC006_100_101	3.42			3.09	13	37	10	362	109	11500	55
LD18RC006_101_102	4.27			1.91	16	64	16	317	95	10750	45
LD18RC006_102_103	7.28			1.06	18	88	15	212	90	4770	22
LD18RC006_103_104	8.14			1.41	20	110	13	285	100	5450	22
LD18RC006_104_105	5.31			1.58	20	134	14	315	95	8150	28
LD18RC006_105_106	2.67			1.68	18	113	20	239	72	8440	50
LD18RC006_106_107	1.455			1.05	21	168	32	161	53	5500	28
LD18RC006_107_108	0.218		3	0.57	13	118	43	116	29	1340	14
LD18RC006_108_109	0.161		2	0.18	10	63	15	53	20	1120	30
LD18RC006_109_110	0.094		1	0.24	7	16	13	52	30	1530	33
LD18RC006_110_111	0.136		1	0.57	6	4	11	35	37	3360	35
LD18RC006_111_112	0.688		1	0.68	4	8	15	21	27	4030	44
LD18RC006_112_113	0.272		1	0.85	3	7	13	25	29	5110	46
LD18RC006_113_114	0.041		3	0.40	9	86	37	65	22	2480	28
LD18RC006_114_115	0.055		3	0.12	8	85	35	102	26	624	16
LD18RC006_115_116	0.081		4	0.11	9	97	34	769	74	525	19
LD18RC006_116_117	0.016		3	0.23	7	55	22	125	38	1270	26
LD18RC006_117_118	0.27		2	0.22	16	90	18	546	81	1220	20
LD18RC006_118_119	1.415	5		0.92	18	25	8	564	113	4200	27

LD18RC006_119_120	2.25		3	1.63	22	22	8	590	96	9040	41
LD18RC006_119_120B	1.75			1.63	22	23	6	534	91	8630	39
LD18RC006_119_120C	0.508		1	0.17	4	7	3	97	21	894	7
LD18RC006_120_121	1.94			1.69	19	13	4	532	103	6910	36
LD18RC006_121_122	1.315			0.93	17	44	9	412	116	5010	28
LD18RC006_122_123	0.976			0.47	13	62	19	348	121	2600	20
LD18RC006_123_124	0.278		4	0.37	9	80	33	77	30	2140	21
LD18RC006_124_125	2.04		1	0.80	17	61	17	242	64	4200	23
LD18RC006_125_126	0.619			0.57	29	7	2	61	23	3720	37
LD18RC006_126_127	0.575		1	0.83	22	33	16	264	80	3680	39
LD18RC006_127_128	0.965		2	0.79	18	9	3	236	62	4360	30
LD18RC006_128_129	1.61		1	1.21	19	13	3	583	100	6190	28
LD18RC006_129_130	1.75		1	1.41	17	17	4	396	106	7410	22
LD18RC006_130_131	1.225		1	0.72	17	26	6	329	87	4340	20
LD18RC006_131_132	0.953			0.24	8	47	15	88	45	1530	20

	Bi	Sb	Tl	Te	Hf	Ta	W	Pb	Th	U
	ppm	ppm	ppm	ppm	ppm	ppm	ppm	ppm	ppm	ppm
LD18RC006_48_49	1.81	0.22	0.27	0.91	0.10	<0.05	3.80	7.40	1.70	3.00
LD18RC006_49_50	2.64	0.24	0.25	1.24	0.10	<0.05	4.70	6.90	0.47	2.60
LD18RC006_50_51	4.60	0.17	0.17	2.17	<0.1	<0.05	7.70	2.70	0.26	1.10
LD18RC006_51_52	8.28	0.22	0.15	3.97	0.40	<0.05	7.20	4.20	1.12	1.60
LD18RC006_52_53	20.50	0.33	0.19	11.85	0.60	0.05	11.50	4.80	2.14	2.50
LD18RC006_53_54	22.20	0.33	0.19	12.20	0.60	0.05	10.80	4.70	2.30	2.60
LD18RC006_54_55	18.15	0.33	0.22	9.79	0.80	0.06	7.60	4.60	2.74	2.80
LD18RC006_55_56	14.90	0.33	0.22	8.11	0.80	0.09	5.40	3.90	3.72	2.90
LD18RC006_56_57	4.50	0.15	0.05	2.37	0.30	<0.05	1.40	1.70	1.28	1.20
LD18RC006_57_58	2.24	0.20	0.15	1.19	1.40	0.13	4.80	2.00	3.59	2.50
LD18RC006_58_59	1.55	0.29	0.34	0.65	3.80	0.67	10.80	2.10	4.92	3.60
LD18RC006_59_60	1.13	0.27	0.48	0.42	3.70	0.63	10.30	2.10	3.69	2.50
LD18RC006_59_60B	1.38	0.24	0.44	0.58	3.40	0.60	9.90	2.10	3.98	2.70
LD18RC006_59_60C	0.06	0.10	<0.02	<0.05	<0.1	<0.05	0.20	0.50	0.12	0.10
LD18RC006_60_61	0.71	0.61	0.48	0.28	3.50	0.68	10.70	2.60	3.96	3.70
LD18RC006_61_62	0.61	0.33	0.48	0.17	3.90	0.67	8.30	2.70	6.62	5.80
LD18RC006_62_63	0.26	0.23	0.17	0.10	3.20	0.39	5.70	2.60	8.21	7.60
LD18RC006_63_64	0.41	0.27	0.26	0.23	4.30	0.66	9.10	3.40	13.35	9.90
LD18RC006_64_65	0.38	0.24	0.26	0.17	4.00	0.65	7.00	3.00	11.10	9.20
LD18RC006_65_66	0.56	0.23	0.25	0.29	4.20	0.62	6.60	3.50	11.20	9.90
LD18RC006_66_67	0.33	0.25	0.23	0.16	4.80	0.70	7.50	3.10	11.20	12.00
LD18RC006_67_68	0.20	0.23	0.20	0.13	4.90	0.73	6.60	2.80	12.00	11.30
LD18RC006_68_69	0.22	0.17	0.21	0.12	4.40	0.67	6.80	2.70	10.20	11.90

LD18RC006_69_70	0.23	0.34	0.20	0.10	4.90	0.82	7.70	2.80	12.10	12.00
LD18RC006_70_71	0.35	0.26	0.17	0.22	3.90	0.72	6.00	2.60	10.10	9.50
LD18RC006_71_72	0.31	0.19	0.18	0.18	4.40	0.78	5.90	3.10	12.15	10.70
LD18RC006_72_73	0.31	0.25	0.16	0.20	4.50	0.74	5.90	3.10	12.30	10.90
LD18RC006_73_74	3.49	0.58	0.26	1.76	3.00	0.52	6.00	6.50	8.86	8.30
LD18RC006_74_75	6.94	0.33	0.19	4.09	0.60	0.05	3.60	5.80	1.32	1.40
LD18RC006_75_76	2.40	0.17	0.12	1.28	1.30	0.16	4.20	2.70	3.47	5.00
LD18RC006_76_77	2.58	0.30	0.27	1.22	1.90	0.23	6.60	4.60	5.04	4.80
LD18RC006_77_78	7.54	0.17	0.13	4.19	0.30	<0.05	2.60	3.50	0.97	1.80
LD18RC006_78_79	4.75	0.13	0.10	2.44	0.20	<0.05	1.70	2.40	1.34	0.90
LD18RC006_79_80	6.42	0.07	0.03	4.35	0.10	<0.05	1.10	1.30	0.39	0.90
LD18RC006_79_80B	5.20	0.08	0.03	3.22	0.10	<0.05	1.30	1.30	0.38	0.80
LD18RC006_79_80C	0.12	0.12	<0.02	0.06	0.10	<0.05	0.40	2.00	0.17	0.20
LD18RC006_80_81	1.60	0.22	0.05	0.87	0.30	<0.05	2.00	2.90	0.95	2.40
LD18RC006_81_82	2.57	0.16	0.03	1.55	0.20	<0.05	1.80	1.40	0.68	1.90
LD18RC006_82_83	3.55	0.23	0.16	1.99	1.50	0.15	5.50	2.30	4.08	4.40
LD18RC006_83_84	3.26	0.21	0.09	1.66	0.80	0.07	5.00	5.10	2.44	2.80
LD18RC006_84_85	2.93	0.10	0.03	1.72	0.10	<0.05	2.30	1.70	0.68	1.80
LD18RC006_85_86	2.24	0.13	0.03	1.39	<0.1	<0.05	4.00	3.60	0.24	0.30
LD18RC006_86_87	5.59	0.07	0.02	3.49	0.10	<0.05	2.00	1.90	0.21	0.20
LD18RC006_87_88	2.80	0.17	0.05	1.74	<0.1	<0.05	5.20	4.20	0.26	0.20
LD18RC006_88_89	4.29	0.33	0.08	2.70	0.10	<0.05	5.50	5.20	0.28	0.20
LD18RC006_89_90	7.44	0.21	0.05	4.38	0.10	<0.05	2.30	4.20	0.43	0.50
LD18RC006_90_91	4.49	0.26	0.10	2.35	0.60	0.07	4.20	3.50	2.59	2.80
LD18RC006_91_92	1.14	0.33	0.69	0.45	3.60	0.49	13.70	1.90	3.15	2.40
LD18RC006_92_93	0.54	0.18	1.33	0.19	4.30	0.70	14.40	1.10	2.35	1.00
LD18RC006_93_94	1.03	0.55	0.50	0.32	3.30	0.47	19.50	3.70	3.10	2.60

LD18RC006_94_95	2.43	0.40	0.38	1.00	1.90	0.21	10.00	8.90	3.25	3.70
LD18RC006_95_96	1.61	0.21	0.19	0.58	1.60	0.17	7.80	3.40	4.37	5.40
LD18RC006_96_97	2.13	0.46	0.25	0.85	2.30	0.24	11.70	30.80	6.82	13.20
LD18RC006_97_98	0.88	0.33	0.18	0.23	2.90	0.30	12.80	3.90	8.90	14.30
LD18RC006_98_99	0.60	0.36	0.20	0.16	2.70	0.30	11.40	6.40	7.52	10.10
LD18RC006_99_100	2.16	0.91	0.31	0.93	1.50	0.13	8.50	11.50	4.24	6.10
LD18RC006_99_100B	2.57	0.83	0.28	1.14	1.10	0.13	7.50	7.20	3.82	5.40
LD18RC006_99_100C	0.08	0.17	0.02	0.05	0.10	<0.05	0.40	<0.5	0.24	0.30
LD18RC006_100_101	7.86	0.98	0.52	3.96	0.90	0.08	4.70	12.50	2.99	4.30
LD18RC006_101_102	6.93	0.61	0.54	3.62	1.60	0.10	6.60	8.90	3.05	5.20
LD18RC006_102_103	10.85	0.43	0.30	6.08	1.70	0.09	7.70	5.70	3.34	3.50
LD18RC006_103_104	13.90	0.38	0.20	8.29	1.40	0.14	18.40	5.30	2.43	2.40
LD18RC006_104_105	8.08	0.32	0.18	5.09	1.40	0.14	18.20	4.20	2.05	2.60
LD18RC006_105_106	5.04	0.46	0.20	2.87	2.00	0.24	14.20	4.50	4.60	4.20
LD18RC006_106_107	3.35	0.53	0.24	1.96	3.20	0.40	18.70	4.00	5.68	5.80
LD18RC006_107_108	0.81	0.31	0.14	0.51	4.40	0.70	14.20	3.20	12.00	10.70
LD18RC006_108_109	0.63	0.20	0.09	0.31	1.40	0.18	9.20	2.60	2.54	2.10
LD18RC006_109_110	0.64	0.15	0.04	0.28	0.40	0.05	4.20	2.60	0.99	0.90
LD18RC006_110_111	0.54	0.11	0.02	0.24	0.10	<0.05	3.20	3.00	0.40	0.20
LD18RC006_111_112	0.25	0.17	0.04	0.11	0.20	<0.05	5.70	3.60	0.23	0.10
LD18RC006_112_113	0.35	0.15	0.04	0.19	0.10	<0.05	4.00	2.80	0.42	0.30
LD18RC006_113_114	0.38	0.21	0.10	0.22	3.70	0.60	11.70	2.90	9.47	8.20
LD18RC006_114_115	0.34	0.20	0.06	0.20	4.00	0.64	9.80	2.90	10.10	9.30
LD18RC006_115_116	0.41	0.25	0.07	0.28	3.30	0.56	12.50	2.50	8.26	7.00
LD18RC006_116_117	0.42	0.15	0.06	0.18	1.30	0.15	8.40	3.00	2.75	1.80
LD18RC006_117_118	2.37	0.13	0.07	1.33	1.80	0.22	15.10	2.30	3.17	1.60
LD18RC006_118_119	6.87	0.23	0.12	3.80	0.50	0.05	4.50	3.80	1.22	1.50

LD18RC006_119_120	5.52	0.26	0.11	2.57	0.60	<0.05	3.50	3.90	1.57	3.40
LD18RC006_119_120B	5.20	0.24	0.10	2.45	0.50	0.05	3.50	3.70	1.39	2.90
LD18RC006_119_120C	1.51	0.09	0.03	0.74	0.10	<0.05	1.00	0.90	0.59	0.40
LD18RC006_120_121	5.53	0.20	0.09	2.39	0.20	<0.05	1.70	4.20	0.83	3.40
LD18RC006_121_122	5.38	0.18	0.10	2.55	0.90	<0.05	4.20	3.60	1.20	2.50
LD18RC006_122_123	3.52	0.18	0.09	1.59	1.60	0.16	12.30	3.40	4.26	4.50
LD18RC006_123_124	0.89	0.17	0.09	0.36	3.40	0.41	18.10	2.70	8.40	7.70
LD18RC006_124_125	3.77	0.23	0.11	1.82	1.90	0.14	8.40	3.00	4.04	6.50
LD18RC006_125_126	0.82	0.08	0.04	0.39	0.10	<0.05	1.00	3.50	0.34	0.40
LD18RC006_126_127	2.95	0.18	0.08	1.41	0.50	<0.05	3.30	3.70	1.44	2.10
LD18RC006_127_128	3.33	0.11	0.04	1.83	0.10	<0.05	2.20	2.50	0.58	0.90
LD18RC006_128_129	4.72	0.15	0.07	2.55	0.30	<0.05	2.60	2.40	0.69	1.70
LD18RC006_129_130	5.38	0.21	0.09	2.78	0.30	<0.05	2.90	2.60	0.82	1.90
LD18RC006_130_131	3.76	0.17	0.07	1.87	0.50	<0.05	3.00	2.30	1.31	3.30
LD18RC006_131_132	1.78	0.20	0.09	0.72	1.20	0.14	5.30	2.70	2.65	3.40

Table 3: Rare Earth Element Data

	La	Ce	Pr	Nd	Sm	Eu	Gd	Tb	Dy	Ho	Y	Er	Tm	Yb	Lu
	ppm	ppm	ppm	ppm	ppm	ppm	ppm	ppm	ppm	ppm	ppm	ppm	ppm	ppm	ppm
LD18RC006_48_49	20.30	33.10	3.41	14.80	4.45	1.01	8.92	1.86	14.95	3.34	100.50	11.20	1.63	10.80	1.35
LD18RC006_49_50	7.40	15.35	1.84	9.40	3.98	1.28	9.30	2.25	18.95	5.11	137.00	16.80	2.41	16.20	2.51
LD18RC006_50_51	4.60	8.41	1.04	4.90	1.89	0.50	4.01	0.99	9.18	2.11	59.00	7.20	1.98	8.65	1.16
LD18RC006_51_52	21.00	35.10	3.64	14.70	3.80	0.89	5.79	1.21	7.27	2.40	57.50	5.95	0.97	6.53	1.01
LD18RC006_52_53	38.40	62.20	6.49	27.20	6.07	1.22	6.84	1.27	13.40	2.31	62.70	6.51	1.07	8.02	1.28
LD18RC006_53_54	36.00	62.20	6.56	27.50	6.44	1.28	12.60	1.26	9.79	2.11	67.60	7.28	1.20	7.42	1.31
LD18RC006_54_55	45.10	76.70	7.95	32.70	7.03	1.35	6.42	1.65	12.15	2.48	53.50	5.53	0.97	7.70	1.05
LD18RC006_55_56	86.00	133.00	14.60	53.70	11.00	1.98	11.15	1.87	10.70	2.41	75.40	7.93	1.27	8.77	1.27
LD18RC006_56_57	37.10	60.60	6.31	27.50	7.49	1.49	11.60	2.26	16.25	3.98	115.00	12.55	2.04	13.55	2.05
LD18RC006_57_58	21.90	38.40	4.21	18.50	4.79	0.92	6.55	1.24	8.62	2.24	73.90	6.85	1.12	7.68	1.19
LD18RC006_58_59	35.40	65.10	7.19	30.20	6.33	1.08	5.00	0.69	3.58	0.70	23.00	2.09	0.46	2.41	0.41
LD18RC006_59_60	26.00	49.20	5.59	24.10	5.37	0.99	4.89	0.69	3.58	0.73	24.60	2.18	0.35	2.48	0.42
LD18RC006_59_60B	31.30	57.30	6.30	26.80	5.97	1.08	5.39	0.82	4.83	1.08	28.90	3.11	0.49	3.39	0.54
LD18RC006_59_60C		0.49	0.06	0.30	0.07	<0.03	0.15	0.03	0.19	0.05	1.30	0.16	0.03	0.22	0.03
LD18RC006_60_61	27.10	53.50	5.90	24.40	5.19	1.00	4.49	0.61	3.21	0.59	17.50	1.76	0.29	2.20	0.36
LD18RC006_61_62	34.80	67.10	7.33	29.50	5.69	1.00	4.35	0.56	2.66	0.49	14.40	1.42	0.24	1.59	0.29
LD18RC006_62_63	37.70	70.50	7.51	29.50	5.43	0.98	4.24	0.56	2.77	0.51	15.40	1.56	0.20	1.47	0.26
LD18RC006_63_64	59.50	112.00	13.35	46.10	8.23	1.33	5.86	0.79	3.56	0.70	21.30	2.01	0.30	2.15	0.33
LD18RC006_64_65	40.10	78.50	8.43	32.40	5.77	0.92	4.26	0.58	2.97	0.61	20.20	1.75	0.28	1.92	0.31
LD18RC006_65_66	48.40	90.50	9.67	37.90	6.74	1.17	5.29	0.73	3.67	0.73	22.70	2.15	0.35	2.38	0.41
LD18RC006_66_67	37.20	72.20	7.81	30.90	5.60	0.99	4.27	0.60	3.32	0.67	21.00	1.98	0.31	2.17	0.34
LD18RC006_67_68	39.50	74.80	7.95	30.40	5.61	0.98	4.12	0.59	3.05	0.65	20.00	1.96	0.30	2.02	0.35
LD18RC006_68_69	32.70	60.30	6.43	25.50	4.67	0.92	4.04	0.62	3.54	0.74	22.30	2.17	0.33	2.22	0.36

LD18RC006_69_70	41.50	76.90	7.89	30.50	5.50	1.02	4.15	0.61	3.39	0.80	21.80	2.10	0.33	2.28	0.37
LD18RC006_70_71	36.60	70.80	7.65	29.50	5.70	1.04	4.37	0.67	3.71	0.76	23.50	2.35	0.38	2.43	0.40
LD18RC006_71_72	51.30	100.00	11.20	40.20	7.10	1.27	5.76	0.81	4.19	0.82	26.70	2.52	0.39	2.74	0.41
LD18RC006_72_73	54.60	104.50	12.40	43.70	7.80	1.36	5.50	0.74	3.91	0.76	25.10	2.27	0.42	2.54	0.38
LD18RC006_73_74	49.00	86.70	9.10	35.20	7.14	1.28	6.65	1.04	6.64	1.55	39.60	4.46	0.66	3.88	0.75
LD18RC006_74_75	23.20	39.90	4.40	19.80	5.68	1.18	7.74	1.48	9.72	2.26	67.50	7.02	1.12	7.19	1.09
LD18RC006_75_76	27.60	49.40	5.79	27.40	8.49	1.79	12.55	2.59	16.75	3.76	112.50	11.05	1.79	11.50	1.69
LD18RC006_76_77	26.10	47.60	5.21	22.20	5.59	1.40	7.37	1.38	9.08	2.00	56.10	5.88	0.90	5.80	0.88
LD18RC006_77_78	24.00	40.80	4.50	19.90	5.44	1.28	7.27	1.33	8.77	2.00	60.10	5.96	0.97	6.27	0.97
LD18RC006_78_79	65.20	112.00	13.30	53.50	15.35	3.00	24.00	4.61	28.70	6.31	188.50	17.95	2.82	18.20	2.38
LD18RC006_79_80	22.10	47.50	6.36	37.70	16.35	3.83	30.30	5.99	40.50	8.84	257.00	25.10	3.97	25.40	3.22
LD18RC006_79_80B	24.40	51.80	6.95	39.40	16.70	3.94	31.50	6.07	45.60	10.55	258.00	26.10	3.97	24.50	3.18
LD18RC006_79_80C	0.90	1.72	0.21	0.90	0.26	0.06	0.42	0.08	0.56	0.13	5.60	0.37	0.06	0.37	0.05
LD18RC006_80_81	31.20	62.80	7.85	41.50	16.35	3.64	27.30	5.61	38.10	8.50	261.00	24.30	4.49	23.10	3.05
LD18RC006_81_82	45.10	85.00	10.60	53.40	18.70	3.85	31.30	5.81	37.00	8.29	236.00	24.00	3.83	25.00	3.21
LD18RC006_82_83	38.20	67.80	7.52	34.30	8.94	1.96	13.35	2.49	16.30	3.94	116.00	12.35	1.69	10.80	1.37
LD18RC006_83_84	40.70	70.30	7.88	36.70	9.06	1.73	9.41	1.57	10.75	2.48	73.10	7.35	1.12	7.81	1.16
LD18RC006_84_85	50.50	88.80	10.80	47.00	14.90	3.15	23.00	4.10	27.60	5.76	189.50	16.80	3.24	18.00	2.48
LD18RC006_85_86	13.00	24.00	2.98	15.40	5.21	1.15	8.18	1.67	12.50	2.77	81.40	9.06	1.56	9.70	1.69
LD18RC006_86_87	22.10	44.40	5.96	32.20	12.60	2.42	18.30	3.84	27.50	6.27	170.50	18.10	2.94	19.60	2.80
LD18RC006_87_88	13.40	24.50	2.85	13.80	4.10	0.98	4.38	0.79	5.28	1.19	31.50	3.56	0.76	3.74	0.55
LD18RC006_88_89	17.90	30.70	3.21	13.80	3.85	0.94	4.43	0.85	4.93	1.35	29.70	3.42	0.52	3.34	0.58
LD18RC006_89_90	31.70	56.60	6.25	29.40	8.51	1.81	10.60	1.78	11.10	2.42	76.00	8.10	1.38	9.28	1.33
LD18RC006_90_91	45.70	82.10	8.84	37.40	9.43	1.95	11.20	1.93	14.35	2.79	85.60	8.42	1.45	9.57	1.35
LD18RC006_91_92	28.70	55.20	6.21	27.00	6.20	1.18	6.60	0.92	4.99	0.94	27.80	4.04	0.42	2.81	0.45
LD18RC006_92_93	20.80	41.60	4.84	21.70	4.97	0.89	4.92	0.65	3.79	0.58	16.00	1.62	0.27	1.92	0.34
LD18RC006_93_94	35.10	63.20	6.69	28.10	6.08	1.27	5.66	0.77	3.91	0.74	21.00	2.01	0.33	2.14	0.36

LD18RC006_94_95	37.20	62.90	6.56	28.30	6.01	1.61	6.87	0.97	5.52	1.22	32.60	3.72	0.46	3.09	0.47
LD18RC006_95_96	43.80	74.10	7.82	32.20	7.07	1.88	7.70	1.11	6.26	1.21	38.40	3.28	0.49	3.13	0.46
LD18RC006_96_97	42.70	75.30	7.73	32.10	6.59	1.46	6.33	0.95	8.95	1.13	30.40	2.97	0.49	3.07	0.47
LD18RC006_97_98	59.30	99.70	10.45	40.40	7.74	1.49	7.42	1.10	5.72	1.17	34.70	3.12	0.48	3.24	0.42
LD18RC006_98_99	42.50	73.60	7.57	31.30	6.84	1.90	7.72	1.20	6.74	1.30	40.50	3.51	0.50	3.09	0.44
LD18RC006_99_100	38.00	63.70	6.54	27.30	5.83	1.31	6.09	0.90	5.13	1.07	30.70	3.14	0.63	3.95	0.48
LD18RC006_99_100B	35.40	59.80	6.19	26.30	5.74	1.29	6.10	0.94	5.20	1.22	39.70	3.10	0.49	3.45	0.54
LD18RC006_99_100C	1.60	2.85	0.33	1.40	0.34	0.08	0.40	0.07	0.41	0.09	2.80	0.26	0.04	0.25	0.03
LD18RC006_100_101	34.10	59.60	6.20	26.80	6.04	1.28	6.28	0.87	5.40	1.44	33.30	3.33	0.52	3.87	0.59
LD18RC006_101_102	31.80	55.90	5.90	25.10	6.20	1.23	6.85	0.88	5.31	1.25	33.20	3.51	0.56	4.19	0.72
LD18RC006_102_103	25.70	44.60	4.78	20.30	4.82	1.02	5.25	0.82	5.19	1.39	31.20	3.47	0.60	4.35	0.69
LD18RC006_103_104	23.90	43.10	4.44	19.60	4.74	1.02	5.20	0.81	6.84	1.14	35.40	3.38	0.55	4.03	0.62
LD18RC006_104_105	23.80	42.40	4.59	20.30	4.78	0.97	5.15	0.82	5.17	1.03	30.60	3.07	0.48	3.14	0.49
LD18RC006_105_106	44.20	76.00	7.73	31.60	6.41	1.11	5.95	0.81	4.67	0.89	26.10	2.61	0.44	2.93	0.61
LD18RC006_106_107	39.40	68.90	7.40	31.00	6.26	1.12	5.71	0.78	4.24	0.86	27.40	2.46	0.40	2.67	0.44
LD18RC006_107_108	59.30	105.50	12.00	42.80	8.17	1.25	6.20	0.80	4.25	0.81	24.80	2.33	0.35	2.54	0.39
LD18RC006_108_109	13.70	26.00	2.61	11.00	2.25	0.44	3.06	0.35	2.08	0.44	14.00	1.38	0.24	1.70	0.53
LD18RC006_109_110	5.70	10.85	1.22	5.00	1.17	0.26	1.20	0.20	1.28	0.28	7.80	1.01	0.20	1.47	0.27
LD18RC006_110_111	2.90	5.33	0.60	2.70	0.73	0.22	0.94	0.17	1.35	0.33	7.90	1.09	0.19	1.86	0.33
LD18RC006_111_112	1.90	3.45	0.38	1.60	0.43	0.13	0.58	0.17	0.69	0.16	5.00	0.56	0.10	0.82	0.16
LD18RC006_112_113	4.50	8.30	0.89	3.80	0.80	0.21	1.01	0.15	0.88	0.22	5.70	0.67	0.11	1.19	0.20
LD18RC006_113_114	31.90	58.00	5.88	24.30	4.46	0.87	4.31	0.54	2.86	0.59	20.90	1.83	0.27	2.15	0.34
LD18RC006_114_115	31.20	60.90	6.11	23.50	4.39	0.81	3.69	0.54	3.04	0.61	18.70	1.86	0.29	2.13	0.31
LD18RC006_115_116	25.60	46.70	4.67	18.80	3.72	0.67	3.29	0.51	2.80	0.56	18.40	2.05	0.25	1.82	0.29
LD18RC006_116_117	5.20	9.64	1.09	4.50	1.04	0.26	1.56	0.26	1.25	0.26	8.20	0.93	0.15	1.22	0.22
LD18RC006_117_118	21.20	38.10	3.85	16.00	3.47	0.66	3.31	0.48	2.43	0.67	14.60	1.74	0.32	2.61	0.36
LD18RC006_118_119	22.50	39.30	4.00	17.70	4.18	0.94	4.40	0.62	3.83	0.84	23.60	2.69	0.67	3.85	0.64

LD18RC006_119_120	28.20	48.90	5.04	22.20	5.00	1.22	5.13	0.86	5.05	1.34	29.20	4.35	0.67	4.90	0.97
LD18RC006_119_120B	28.10	48.70	4.98	22.00	5.17	1.22	5.43	0.81	4.61	1.09	31.80	4.00	0.65	5.05	0.87
LD18RC006_119_120C	5.30	10.55	1.12	4.70	1.10	0.28	1.38	0.26	1.68	0.40	10.70	1.22	0.19	1.39	0.21
LD18RC006_120_121	15.70	27.50	2.78	12.70	3.31	0.90	4.22	0.67	4.05	0.97	28.80	2.92	0.51	4.79	0.91
LD18RC006_121_122	17.10	30.70	3.17	14.20	3.58	0.78	4.12	0.67	4.28	1.07	28.60	3.85	0.66	5.01	0.78
LD18RC006_122_123	34.20	59.40	5.96	24.90	5.20	0.97	4.87	0.72	4.13	0.91	25.00	3.22	0.41	3.24	0.54
LD18RC006_123_124	68.20	118.50	12.60	46.20	8.44	1.44	6.69	0.91	4.16	0.82	24.20	2.19	0.34	2.39	0.37
LD18RC006_124_125	20.00	37.00	3.85	17.10	4.61	0.98	5.26	0.82	5.34	1.21	34.80	4.00	0.63	5.09	0.79
LD18RC006_125_126	13.20	24.10	2.60	12.20	3.85	1.15	5.68	1.01	7.48	1.58	44.40	5.49	1.71	7.32	1.29
LD18RC006_126_127	16.90	30.40	3.18	14.30	3.87	0.95	4.76	0.81	5.22	1.27	34.30	3.78	0.63	5.04	0.78
LD18RC006_127_128	10.20	20.70	2.20	10.70	3.30	0.85	5.13	1.00	7.35	1.68	49.70	5.85	0.96	7.43	1.10
LD18RC006_128_129	16.90	31.10	3.20	14.40	3.89	1.04	4.30	1.00	5.10	1.64	35.40	4.31	0.64	5.62	0.98
LD18RC006_129_130	17.20	31.40	3.30	14.90	4.43	1.06	4.15	0.77	5.57	0.98	26.90	3.21	0.54	4.60	0.78
LD18RC006_130_131	28.70	50.40	5.08	21.50	4.73	0.96	4.79	0.84	4.49	1.00	54.10	3.95	0.55	4.43	0.72
LD18RC006_131_132	12.90	24.60	2.56	11.60	2.70	0.86	3.70	0.69	3.83	0.86	22.60	2.78	0.45	3.66	0.54

Table 4: Key Element Ratios

	Y/Ho	Zr/Hf	La/Yb	TREE	Molar Cu/Au	Ag/Au
LD18RC006_48_49	30.09	39.00	1.88	131.12	111244	5.89
LD18RC006_49_50	26.81	35.00	0.46	112.78	67605	3.48
LD18RC006_50_51	27.96		0.53	56.62	31166	1.85
LD18RC006_51_52	23.96	38.50	3.22	110.26	12228	0.59
LD18RC006_52_53	27.14	37.00	4.79	182.28	10734	0.56
LD18RC006_53_54	32.04	49.50	4.85	182.95	9199	0.60
LD18RC006_54_55	21.57	36.50	5.86	208.78	10166	0.58
LD18RC006_55_56	31.29	41.63	9.81	345.65	9508	0.55
LD18RC006_56_57	28.89	30.00	2.74	204.77	16747	0.99
LD18RC006_57_58	32.99	36.86	2.85	124.21	6588	0.34
LD18RC006_58_59	32.86	37.24	14.69	160.64	27746	1.57
LD18RC006_59_60	33.70	38.38	10.48	126.57	26919	1.37
LD18RC006_59_60B	26.76	38.82	9.23	148.40		1.25
LD18RC006_59_60C	26.00		0.00	1.78		5.00
LD18RC006_60_61	29.66	38.43	12.32	130.60	27390	1.63
LD18RC006_61_62	29.39	38.33	21.89	157.02	36677	2.08
LD18RC006_62_63	30.20	38.59	25.65	163.19	58115	3.75
LD18RC006_63_64	30.43	38.72	27.67	256.21	16513	1.03
LD18RC006_64_65	33.11	37.88	20.89	178.80	5057	0.39
LD18RC006_65_66	31.10	39.17	20.34	210.09	49849	3.33
LD18RC006_66_67	31.34	36.98	17.14	168.36	25667	2.50
LD18RC006_67_68	30.77	37.35	19.55	172.28	24214	1.88
LD18RC006_68_69	30.14	37.39	14.73	144.54	2441	0.21
LD18RC006_69_70	27.25	35.00	18.20	177.34	142738	5.79
LD18RC006_70_71	30.92	39.49	15.06	166.36	26242	2.00
LD18RC006_71_72	32.56	36.59	18.72	228.71	42728	2.86
LD18RC006_72_73	33.03	38.33	21.50	240.88	26500	4.00
LD18RC006_73_74	25.55	39.67	12.63	214.05	13569	0.79
LD18RC006_74_75	29.87	29.33	3.23	131.78	16963	0.97
LD18RC006_75_76	29.92	35.85	2.40	182.15	10219	0.91
LD18RC006_76_77	28.05	35.11	4.50	141.39	9114	0.63
LD18RC006_77_78	30.05	32.00	3.83	129.46	4443	0.25
LD18RC006_78_79	29.87	41.00	3.58	367.32	5317	0.36
LD18RC006_79_80	29.07	46.00	0.87	277.16	14812	0.88
LD18RC006_79_80B	24.45	53.00	1.00	294.66		0.84
LD18RC006_79_80C	43.08	25.00	2.43	6.09		2.50
LD18RC006_80_81	30.71	32.33	1.35	297.79	8142	0.95
LD18RC006_81_82	28.47	28.50	1.80	355.09	5180	0.58

LD18RC006_82_83	29.44	37.00	3.54	221.01	14480	1.13
LD18RC006_83_84	29.48	36.13	5.21	208.02	5504	0.36
LD18RC006_84_85	32.90	48.00	2.81	316.13	5438	0.31
LD18RC006_85_86	29.39		1.34	108.87	22931	1.35
LD18RC006_86_87	27.19	11.00	1.13	219.03	7698	0.41
LD18RC006_87_88	26.47		3.58	79.88	48488	2.52
LD18RC006_88_89	22.00	41.00	5.36	89.82	29615	1.49
LD18RC006_89_90	31.40	21.00	3.42	180.26	10169	0.55
LD18RC006_90_91	30.68	42.50	4.78	236.48	11290	0.62
LD18RC006_91_92	29.57	37.92	10.21	145.66	7749	0.36
LD18RC006_92_93	27.59	40.12	10.83	108.89	60568	3.33
LD18RC006_93_94	28.38	38.18	16.40	156.36	43485	2.44
LD18RC006_94_95	26.72	38.53	12.04	164.90	10617	0.60
LD18RC006_95_96	31.74	40.56	13.99	190.51	14534	0.72
LD18RC006_96_97	26.90	37.04	13.91	190.24	14436	0.84
LD18RC006_97_98	29.66	36.55	18.30	241.75	12095	1.63
LD18RC006_98_99	31.15	38.89	13.75	188.21	36615	2.67
LD18RC006_99_100	28.69	34.53	9.62	164.07	17762	1.17
LD18RC006_99_100B	32.54	39.36	10.26	155.76		1.18
LD18RC006_99_100C	31.11	41.00	6.40	8.15		1.56
LD18RC006_100_101	23.13	35.44	8.81	156.32	10422	0.90
LD18RC006_101_102	26.56	36.06	7.59	149.40	7803	0.45
LD18RC006_102_103	22.45	37.12	5.91	122.98	2031	0.15
LD18RC006_103_104	31.05	36.07	5.93	119.37	2075	0.17
LD18RC006_104_105	29.71	38.14	7.58	116.19	4757	0.30
LD18RC006_105_106	29.33	37.15	15.09	185.96	9798	0.63
LD18RC006_106_107	31.86	37.50	14.76	171.64	11716	0.72
LD18RC006_107_108	30.62	39.20	23.35	246.69	19052	2.61
LD18RC006_108_109	31.82	35.71	8.06	65.78	21561	1.12
LD18RC006_109_110	27.86	37.25	3.88	30.11	50448	2.55
LD18RC006_110_111	23.94	34.00	1.56	18.74	76575	4.19
LD18RC006_111_112	31.25	26.00	2.32	11.13	18155	0.99
LD18RC006_112_113	25.91	47.00	3.78	22.93	58229	3.13
LD18RC006_113_114	35.42	36.76	14.84	138.30	187479	9.76
LD18RC006_114_115	30.66	37.75	14.65	139.38	35165	2.18
LD18RC006_115_116	32.86	35.76	14.07	111.73	20089	1.36
LD18RC006_116_117	31.54	37.46	4.26	27.58	246019	14.38
LD18RC006_117_118	21.79	38.94	8.12	95.20	14005	0.81
LD18RC006_118_119	28.10	40.00	5.84	106.16	9200	0.65
LD18RC006_119_120	21.79	34.33	5.76	133.83	12453	0.72
LD18RC006_119_120B	29.17	39.20	5.56	132.68		0.93

LD18RC006_119_120C	26.75	55.00	3.81	29.78		0.33
LD18RC006_120_121	29.69	39.50	3.28	81.93	11040	0.87
LD18RC006_121_122	26.73	37.22	3.41	89.97	11809	0.71
LD18RC006_122_123	27.47	39.13	10.56	148.67	8257	0.48
LD18RC006_123_124	29.51	36.32	28.54	273.25	23859	1.33
LD18RC006_124_125	28.76	36.89	3.93	106.68	6381	0.39
LD18RC006_125_126	28.10	40.00	1.80	88.66	18627	0.92
LD18RC006_126_127	27.01	37.80	3.35	91.89	19836	1.44
LD18RC006_127_128	29.58	50.00	1.37	78.45	14004	0.82
LD18RC006_128_129	21.59	27.33	3.01	94.12	11917	0.75
LD18RC006_129_130	27.45	38.00	3.74	92.89	13124	0.81
LD18RC006_130_131	54.10	38.60	6.48	132.14	10981	0.59
LD18RC006_131_132	26.28	35.92	3.52	71.73	4976	0.25

4.1 Trace Element Abundances

4.1.1 Nickel, Cobalt Copper and Arsenic

Selected trace element abundances and elemental ratios for Little Duke RC assays are given in (Tables 2 to 4). Figure 2 shows that transition metals, Ni Co and Cu are positively correlated, ranging up to 10,000 ppm Cu, ~200 ppm Ni and ~ 1000 ppm Co (Figure 2a, b & d). Arsenic is also positively correlated with Co (Figure 2c) which suggests the possible presence of cobaltite in the mineral system. Such positive covariations indicate a genetic relationship, that is interpreted to reflect the role of olivine fractionation in the ultramafic to mafic igneous source of the hydrothermal fluids responsible for formation of the Little Duke breccia system.

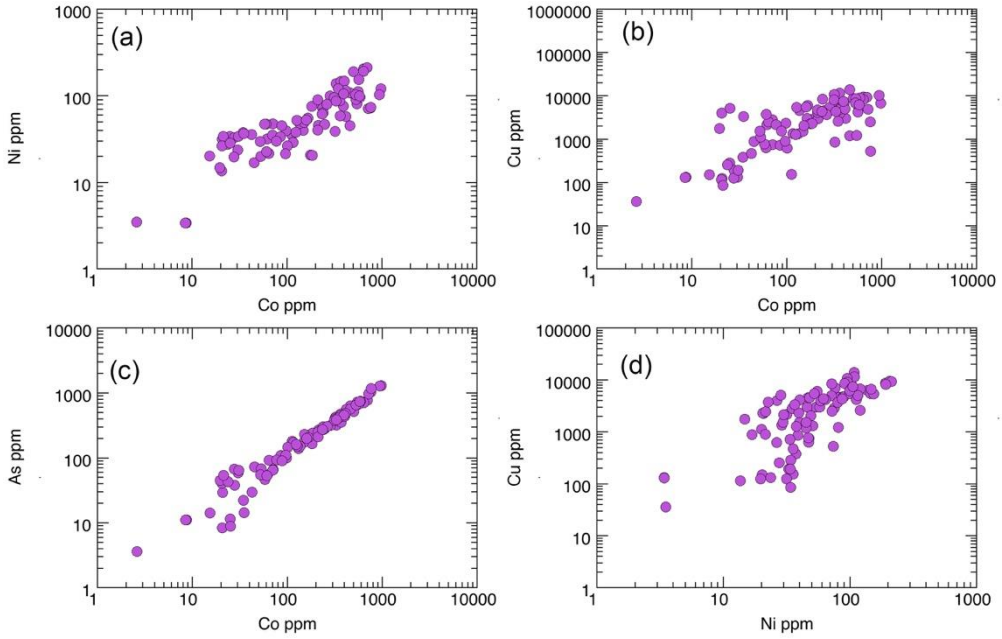

Figure 2: Covariation between (a) Ni and Co, (b) Cu and Co, (c) As and Co and between Cu and Ni.

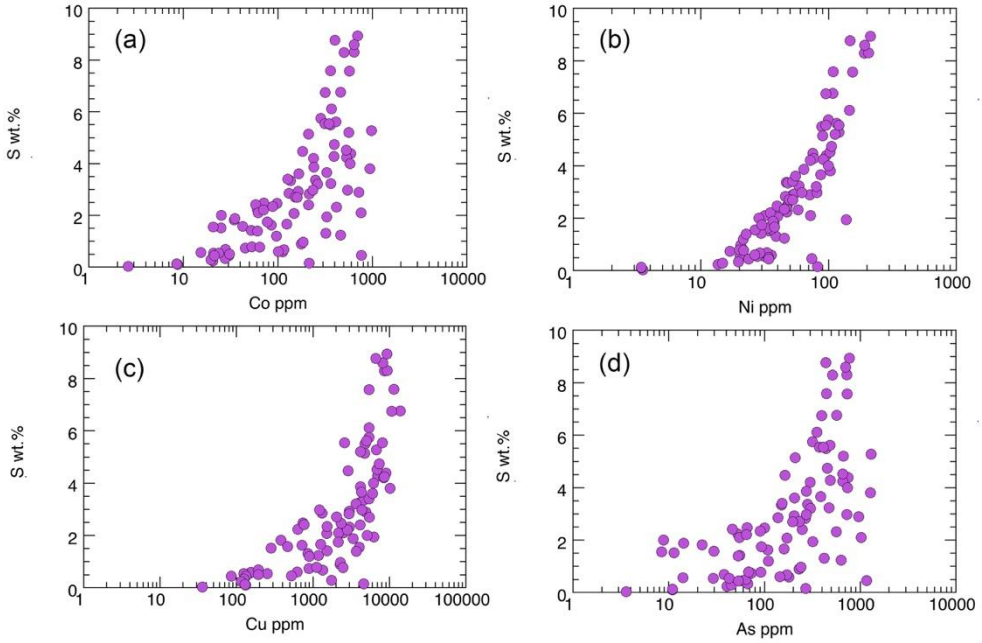

Figure 3: Covariation between (a) Co, (b) Ni (c) Cu and (d) As with S. This strongly suggests the impact of sulphide fractionation in the Little Duke mineral system.

Importantly, the covariation between (a) Co, (b) Ni (c) Cu and (d) As with S shown in Figure 3, indicates that sulphide fractionation also occurred during the evolution of the Little Duke mineral system.

Figure 4 shows that the system was relatively Zn-poor and that its geochemical behavior was largely independent of S, Co or Cu.

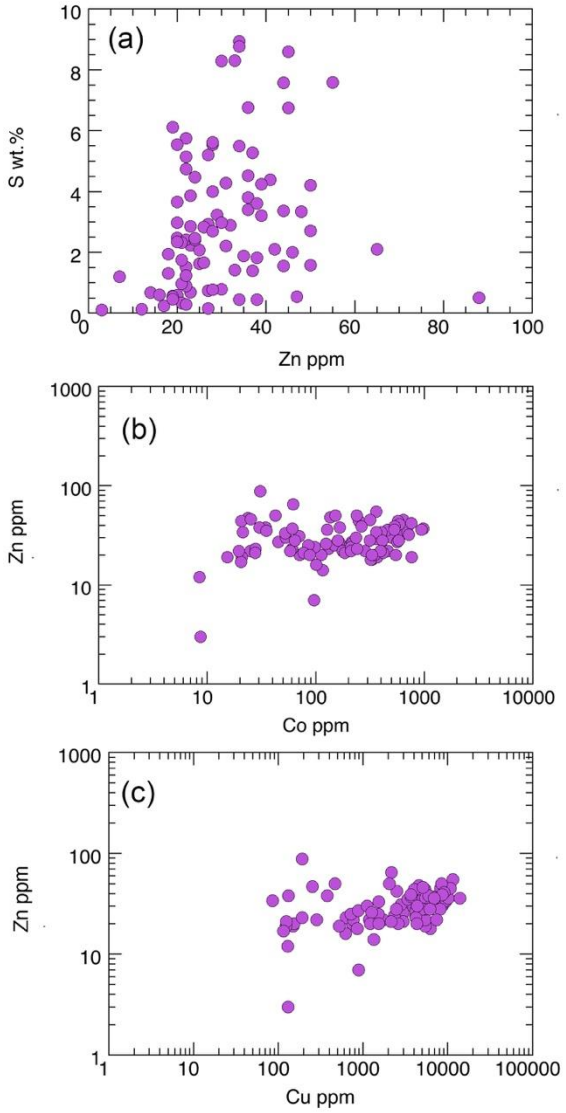

Figure 4: Covariation between (a) S and Zn, (b) Zn and Co and (c) Zn and Cu

4.1.2 Gold

Table 2 and Figure 5 show that the Little Duke breccia system is very Au-rich, containing samples with up to 8 ppm (g/t) Au.

Importantly, Au abundances are extremely well correlated with Te, Bi and Sb (Figure 5) . Figures 5 a and b show two Au enrichment trends that are correlated with Te and Bi. This is interpreted to indicate the effect of several hydrothermal enrichment events in the Little Duke breccia system, one that that resulted in grades of ~ 8 g/t, the other yielding grades of ~ 3 g/t. Data in Figure 5c shows that fluids associated with this lower grade event contained slightly elevated Sb.

As similar systematics in other epithermal systems have been interpreted to indicate that Au transport and concentration is associated with volatiles derived from a proximal igneous source (Marinova et al., 2013), this could have important implications for proximity of a large IOCG mineral system below Little Duke.

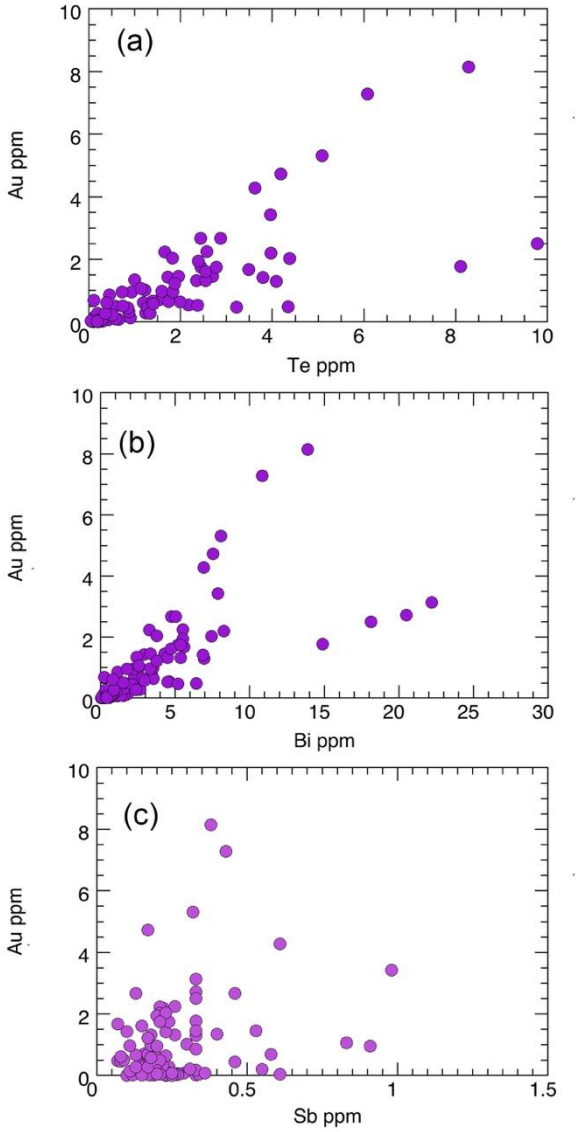

Figure 5: Covariation between Au and (a) Te, (b)Bi and (c) Sb

4.1.3 Ag/Au Systematics

The log normal distribution Ag/Au ratios shown in Figure 6 indicates precious metal transport occurred in boiling solutions (Cole and Drummond 1986). More intense zones of gold and silver enrichment generally occur near the top of the boiling interval which may be analogous to the very high-grade bonanza ores observed in many precious metal vein deposits. Such a distribution is typical of epithermal Au and Ag systems worldwide.

Importantly, this interpretation is supported by petrographic evidence presented in Collerson (2018) regarding the role of high level boiling fluids in formation of Au mineralisation occurring between Guilded Rose and Mount Freda (Figure 1).

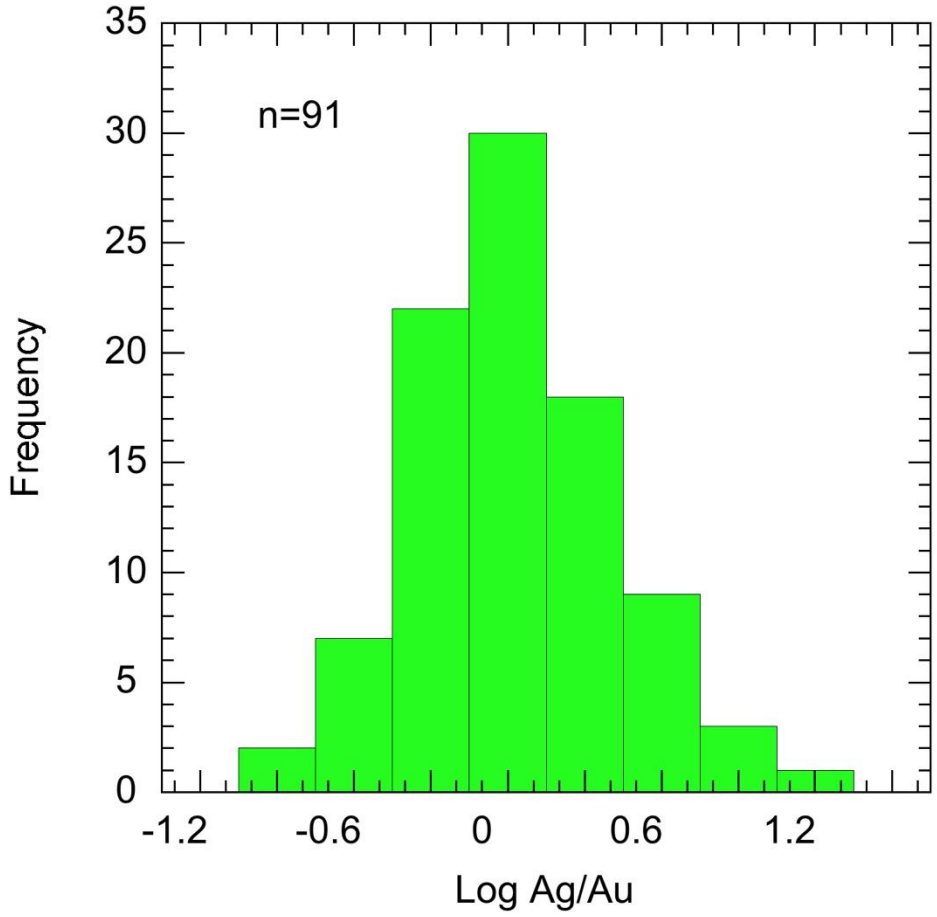

Figure 6: Log normal distribution for Ag/Au at Little Duke is typical of epithermal Au Au hydrothermal systems

4.4 Rare Earth Element Systematics

4.4.1 Chondrite Normalised Plots

In nature REEs with even-atomic numbers are more abundant than the adjacent REE odd-atomic numbered REEs. This reflects the "Oddo-Harkins Rule" caused by differences in binding energies and thus relative stabilities of nuclei with paired and unpaired nucleons. To overcome this situation, REE abundances are normalised to REE abundances in chondritic meteorites, such as C1 chondrites - the composition of the solar nebular from which the Earth accreted (Anders and Grevesse, 1989). These normalised REE data are then arranged in order of increasing atomic numbers, from La to Lu and plotted on a logarithmic scale.

Note to be ore-grade hard rock deposits must have LREE (La to Eu) abundances that >1000 to 10000 chondritic levels and the HREE (Gd to Lu) abundances > 1000 times chondrites.

Chondrite normalised REE data using normalizing data from McDonough and Sun (1995) for selected samples with highest REE abundances in Table 3 are plotted in Figures 7.

Maximum REE and Y contents range from 827 to 744 ppm (in LD18RC006 between 78 and 82 m).

Most samples in Figure 7 have slightly fractionated LREEs and unfractionated HREE reaching ~ 100 to 200 x chondrites. They have pronounced negative Eu anomalies which indicates either feldspar or fluorite fractionation. The positive Y anomaly exhibited by some samples (e.g., LD18RC006 - 71-72, 72-73, 79-80c, 88-89 and 89-90) indicates the effect of fluorine induced fractionation of Y from Ho (Bau and Dulski, 1995; Buhn, 2008). This has implications for understanding the chemistry of hydrothermal systems and also the character of the igneous source.

Chondrite normalized patterns shown in Figure 7, are broadly similar to those exhibited by alkaline syenites, monzonites, diorites and gabbros. Furthermore, the unfractionated HRE patterns at ~ 100x chondrites, indicates the likely effect of a HREE-mineral phase, possibly xenotime. However, this would need to be established via a mineral chemical study.

In view of the halogen rich nature of the hydrothermal system responsible for formation of the Little Duke breccia, potential exists at Little Duke for higher concentrations of HREEs in a proximal aureole to the hydrothermal breccia system.

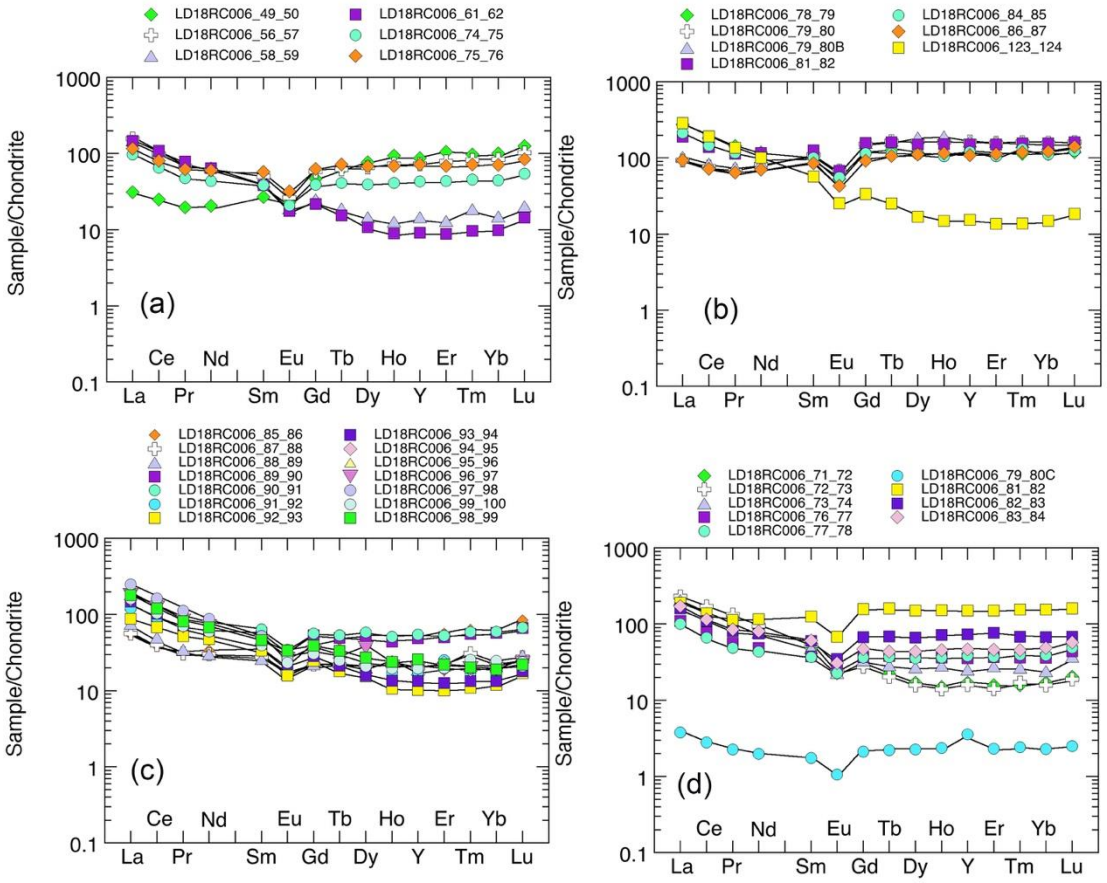

Figure 7: Chondrite normalized REE plots for representative REE-rich samples from Little Duke

4.4.2 La/Yb versus Total Rare Earth Discrimination Projection

La/Yb (a proxy for LREE/HREE ratio) plotted against total REE concentrations is a very useful diagram to discriminate between REE sources (Loubert *et al.,* 1972). In Figure 8 the position of Little Duke RC assays shows that the REEs in the mineral system were derived from a fractionated alkaline source. Importantly, data for one of the chip samples reported in Collerson (2018) is has higher REE abundances and falls within the hydrothermal enrichment field. It is such hydrothermal compositions with >1000 ppm REEs and La/Yb rations <1, that are highly prized as HREE exploration targets.

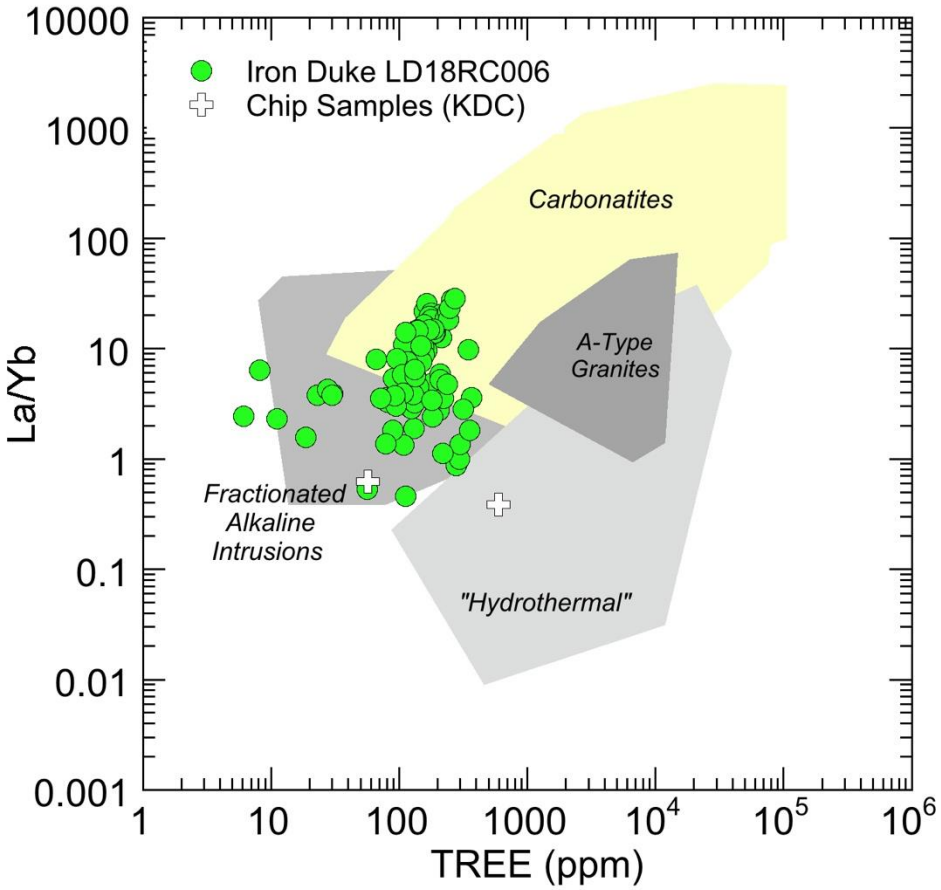

Figure 8: La/Yb versus TREE plot showing data obtained in this study.

4.4.3 CHARAC Ratio Systematics

Ratios of the high field strength elements Zr and Hf, as well as Y and the heavy rare earth element Ho, are useful to evaluate the nature of hydrothermal processes in mineral systems. These so called CHARAC ratios (Y/Ho and Zr/Hf) enable magmatic source characteristics in mineral deposits to be distinguished from systems affected by hydrothermal processes (Bau, 1996).

If a mineral system is characterized by CHArge and-RAdius-Controlled (CHARAC) trace element behaviour, elements with similar charge and ionic radius, such as the twin pairs Y-Ho and Zr-Hf, should display coherent behaviour during crystallization and retain their respective chondritic ratios. Mantle-derived igneous

rocks, for example, have Y/Ho and Zr/Hf ratios close to the ratios recorded by chondritic meteorites, viz. 28 and 38. Carbonatites and alkaline igneous systems display this characteristic (de Andrade et al., 2002).

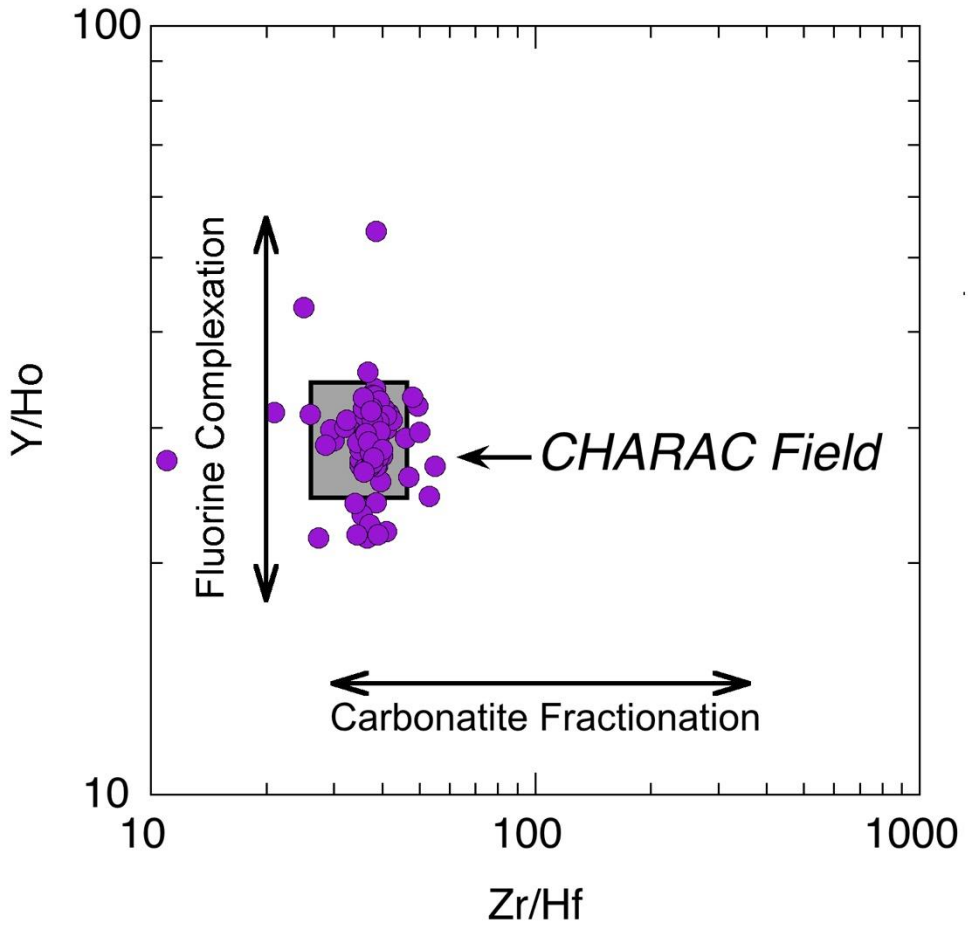

Figure 9: CHARAC ratio plot showing that samples from Little Duke chondritic Zr/Hf but with non-chondritic Y/Ho ratios that plot outside the CHARAC field. This is due to the effect of F fractionation.

These ratios are within error of values exhibited by mantle plume generated ocean island basalts (OIBs) viz., Y/Ho = 27.7±2.7 and Zr/Hf = 36.6.±2.9 (Bau, 1996). Thus, they are useful indicators of mantle plume magmatism.

The spread in Y/Ho ratios show that Y can be fractionated from Ho due to fluoride complexation in medium-temperature F-rich aqueous fluids (Bau and Dulski, 1995; Buhn, 2008). The presence of sub-and super-chondritic Y/Ho ratios indicates the involvement of halogen-rich hydrothermal fluids in the evolution of cobalt and REE-bearing mineral system at Little Duke.

4.5 Molar Cu/Au Systematics

Cu/Au ratios and bulk metal contents, specifically Au grades are controlled by magmatic chemistries (Sillitoe 1997, Halter et al., 2002; Heinrich, et al., 2005) as well as fluid phases separation into brine and vapour which results in Cu-Au fractionation into vapour and possibly to partial separation of the two metals (Simon et al., 2005,

Heinrich et al.,1999; 2005, Pokrovski et al., 2008). Final ore grades are however controlled by precipitation efficiency of Cu-sulphides and native Au during cooling (Ulrich et al., 2001).

Molar Cu/Au ratios are thus believed to be controlled initially by magma source chemistries and subsequently by the physical-chemical evolution of the ore forming hydrothermal fluids.

The histogram of molar Cu/Au ratios calculated for Little Duke assays (Table 4) are shown in Figure 10. The majority of samples have molar Cu/Au ratios between ~10,000 and 50,000. As this range is characteristic of alkaline igneous systems, it further confirms the affinity of the possible IOCG igneous system below Little Duke.

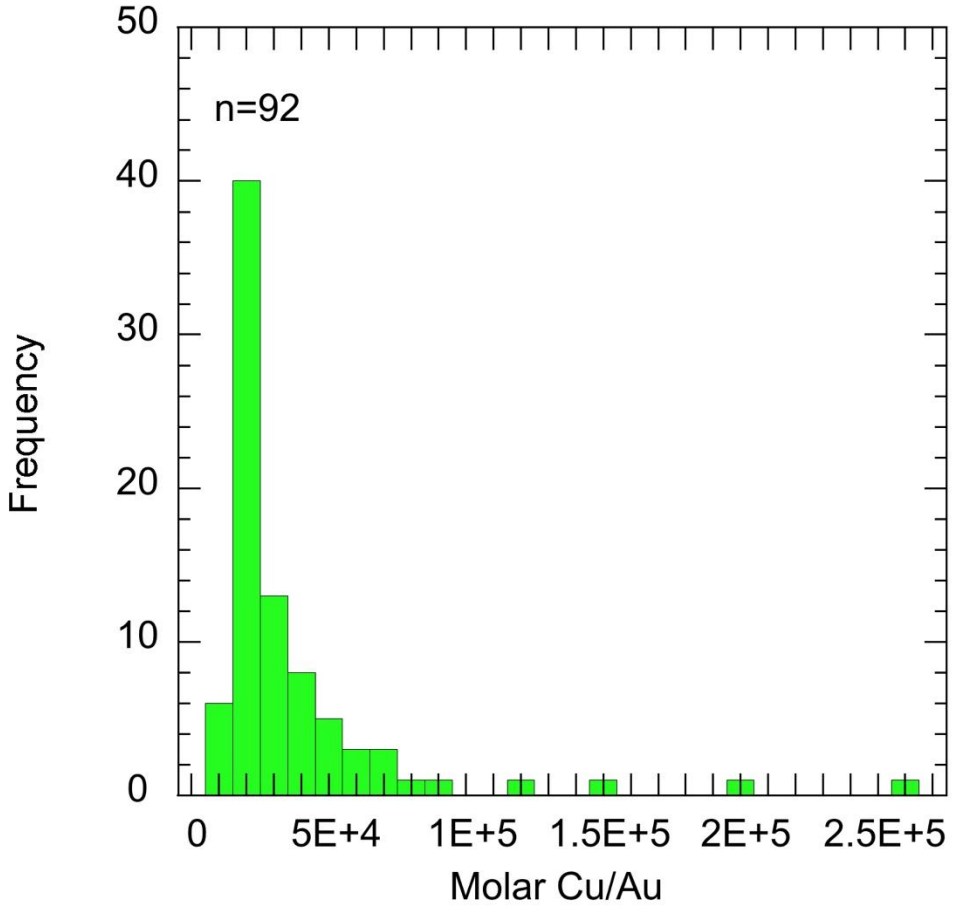

Figure 10: **Histograms showing molar Cu/Au ratios for Little Duke samples**

4.6 Highly Siderophile Elements (HSE)

4.6.1 Background

Unlike the lithophile elements e.g., Sc, REEs, Mn, V and Cr, that occur at chondrite concentration levels in the l mantle, the PGEs, Re, and Au are strongly siderophile "iron-loving elements," and are depleted by two orders-of-magnitude relative to chondritic meteorites in the terrestrial mantle (Mungall and Naldrett, 2008; Lorand et al., 2008). Thus, the concentration of PGEs in the silicate Earth is about 0.023 ppm (Table 5) and the major PGE reservoir is the core, which contains 16,240 ppm total PGEs and 500 ppb Au (Table 14).

Given the above geochemical constraints, for PGE ores to be worth mining, they must contain at least 4 ppm (Mungall and Naldrett, (2008). This represents a significant enrichment over typical crustal rock values. Sulfur controls the genesis of PGE deposits. Firstly, the presence of sulfide as a residual phase during mantle melting limits the availability of PGE to magmas. Secondly, to form of a PGE ore deposit requires the saturation of magma with immiscible sulfide liquid and the collection of that liquid in structural traps within magmatic systems.

Table 5: PGE and gold abundances in terrestrial reservoirs. After McDonough and Sun (1995)

	Chondrite	Bulk Earth	Core	Pyrolite	Bulk Silicate
Os (ppb)	490	900	2800	3.4	3
Ir (ppb)	455	900	2600	3.2	3
Ru (ppb)	710	1300	1300	5	5
Rh (ppb)	130	240	740	0.9	1
Pt (ppb)	1010	1900	5700	7.1	7
Pd (ppb)	550	1000	3100	3.9	4
Au (ppb)	140	1600	500	1	1
Total PGEs (ppb)	3345	6240	16240	23.5	23
Total PGEs (ppm)	3.345	6.24	16.24	0.0235	0.023

4.6.2 Highly Siderophile Element (HSE) Abundances

HSE abundances are given in Table 2. Au is enriched in Little Duke samples with a maximum of ~ 8 ppm (8 g/y) Likewise Pd is also enriched with maximum Pt and Pd values are 112 ppb and 160 ppb.

To assist in comparing the source of the HSEs, primitive mantle normalized HSE abundances plots are shown on Figures 11. The elevated Au values are interpreted reflect the role epithermal enrichment. Note the Mary Kathleen mineral system shows a similar fractionation pattern suggesting the involvement of a similar mafic/ultramafic alkaline source for both mineral systems. Given this similarity, it is considered highly

improbable that any of the HSEs in the Cloncurry Belt IOCG systems were derived from an alkaline granitic source (cf., Kendrick et al., 2007, Williams et al., (2015).

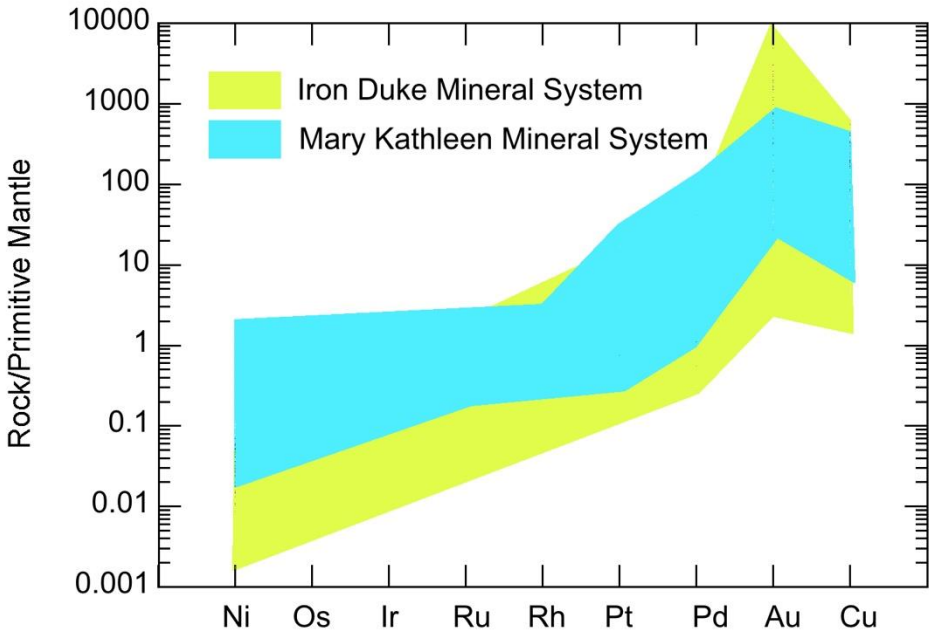

Figure 11: Primitive mantle normalized HSE abundances plots for Little Duke. Note the Mary Kathleen mineral system shows a similar fractionation pattern suggesting the involvement of a similar composition mafic/ultramafic alkaline source.

5. Co-REE Bearing IOCG System in the Eastern Succession

The geodynamic framework for ~1590 Ma magmatism that generated the Olympic Dam deposit (Johnson and Cross, 1995) is interpreted to have involved an upwelling Mesoprotersoic mantle plume (Betts et al., 2007, 2009) during fragmentation of the supercontinent Columbia.

This deep-sourced upwelling plume delivered metals, a flux of volatiles enriched in fluorine (Marks et al., 2014), and also heat for crustal melting to form the Gairdner Large Igneous Province (LIP) containing the Gawler Range Volcanics and emplacement of the Hiltaba Granites.

This halogen enriched fluid played a crucial role in metal transport during formation of the Olympic Dam deposit (McPhie et al., 2011). For example, fluorine-rich hydrothermal fluids are interpreted to have been responsible for the high metal content (including REEs) of the Olympic Dam deposit and they were crucial in enabling development of its polymetallic character. As a result, the mineralisation is enriched in fluorine and there is an intimate association between Cu sulphides and fluorite in the hematite-rich breccias (Roberts and Hudson, 1983; Oreskes and Einaudi, 1990; Haynes et al., 1995).

The same Mesoproterosoic plume magmatic event was also responsible for IOCG and Cu-Au-U-REE mineralisation in the Eastern Succession and the Mary Kathleen Belt ~1.55 - 1.5 Ga (Collerson, 2018, Duncan et al., 2011).

A large magnetotelluric conductive anomaly has recently been reported to occur below the Ernest Henry IOCG deposit (Wang et al., 2018). An image of this anomaly is shown in Figure 12. Importantly a similar conductive anomaly also occurs below Olympic Dam deposit where it has been interpreted to image the lithospheric response of the metal migration regime associated with this plume generated world class IOCG system (Heinson et al., 2018). Thus, it is likely that the same fluorine-rich and oxidizing hydrothermal fluids that formed the Olympic Dam IOCG deposits remained active as the plume track migrated to the north east and generated the Cloncurry Belt IOCG mineralisation.

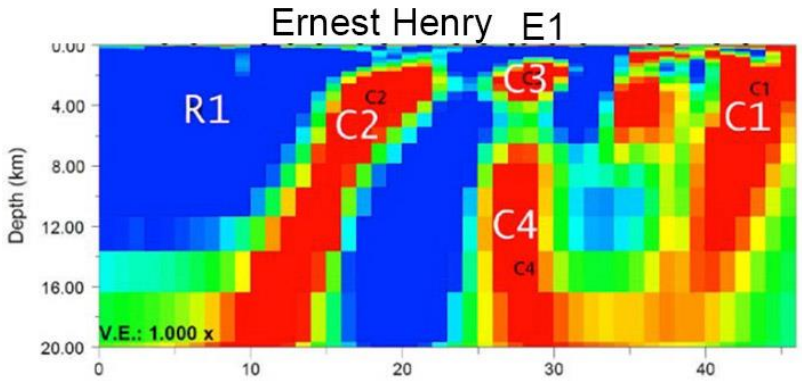

Figure 12: Deep penetrating MT Conductive anomalies below Ernest Henry and the E1 IOCG Deposits.

6. Summary and Recommendations

- The Little Duke breccia system is a high level epithermal system that is proximal to am ultramafic to mafic igneous source of halogen-rich fluids and metals that include Co, Ni, Cu, As, Au, Ag, PGEs.
- Although earlier studies of the IOCG mineral system in the Cloncurry area suggested that Cu, Au, F, U, P and REEs as well as S were derived from the Williams Naraku Granite via a magmatic-hydrothermal fluid (Williams et al., 2015), given the element association (Co, Ni, PGE's and Au), a more plausible explanation is that metals in the system were derived from an ultramafic to mafic alkaline igneous source.
- High levels of positively correlated Ni, Co and Cu confirm the role of olivine fraction in the igneous source of the Little Duke breccia. This metal association simply cannot be explained by a granitic source.
- Positively correlated S with Ni, Co, Cu and As also confirms the involvement of magmatic/hydrothermal processes below Little Duke.
- Correlations between Te, Bi and Sb with Au, indicates that the breccia system is proximal to the igneous source of the Little Duke mineral system.
- Halogen-rich fluids that form halogen complexes are conducive to fluid - metal transport. These were operative at Little Duke where dissociation of these complexes occured in response to changes of the hydrothermal environment such as fluid–rock interaction, fluid mixing, cooling, and phase separation.
- Molar Cu/Au ratios are controlled initially by magma source chemistries and subsequently by the physical-chemical evolution of the ore forming hydrothermal fluids. Little Duke samples with molar Cu/Au ratios between ~30,000 and 100,000 are typical of alkaline igneous systems.
- La/Yb - HREE systematics also support an ultramafic to mafic igneous source and suggest the possible presence of HREE enriched alteration haloes proximal to the Little Duke breccia system.
- Sub-and super-chondritic Y/Ho ratios indicates the involvement of halogen-rich hydrothermal fluids in the Little Duke breccia system.
- Primitive mantle normalized highly siderophile element abundance (Ni, PGE, Au and Cu) plots exhibit similar levels of enrichment and fractionation patterns to deposits in the Mary Kathleen Belt. This suggests that both Cloncurry belt and the adjacent Mary Kathleen Belt were influenced by the same metal fertile plume magmatic source. Given this similarity, it is considered highly improbable that any of the HSEs were derived from an alkaline granitic source as suggested by Kendrick et al., (2007) and Williams et al., (2015).
- The presence of a log normal Ag/Au distribution reflects precious metal transport in boiling solutions, confirming a high level epithermal depositional environment associated with hot springs (Cole and Drummond, 1986).
- The epithermal deposits along the Golden Mile, from Guilded Rose to Mount Freda are Au rich. Covariation of Au with Bi and Te indicates the close relationship to an igneous source (Marinova et al., 2013).
- The presence of these features indicates that hot springs occurred above IOCG source intrusions in the Cloncurry area and explains the occurrence of high concentrations of Au in the district.

- Little Duke data are highly significant and it is recommended that diamond core drilling should continue in the RC holes to target the deeper source IOCG or ISCG alkaline igneous of the metal anomalism reported to date in the RC assays.
- The presence of a large magnetotelluric conductive anomaly below the Ernest Henry IOCG deposit (Wang et al., 2018) is similar to the MT anomaly below Olympic Dam and likely reflects the lithospheric response of the metal migration regime associated with this plume generated world class IOCG system (Heinson et al., 2018).
- Thus it is likely that the same fluorine-rich and oxidizing hydrothermal fluids that formed the Olympic Dam IOCG deposits remained active as the plume track migrated to the north east and generated the Cloncurry Belt IOCG mineralisation.
- The data indicate that Little Duke is likely to be proximal to a deeper and fertile IOCG mineral system, that could be confirmed by deeper drilling.

7. References

Anders, E., Grevesse, N. (1989) Abundances of the elements: Meteoritic and solar. *Geochim. Cosmochimica Acta* 53: 197-214.

Bau M. (1996) Controls on the fractionation of isovalent trace elements in magmatic and aqueous systems: Evidence from Y/Ho, Zr/Hf, and lanthanide tetrad effect. *Contrib. Mineral. Petrol.* 123: 323-333.

Bau, M., Dulski, P. (1995) Comparative study of yttrium and rare-earth element behaviours in fluorine-rich hydrothermal fluids. *Contrib. Mineral. Petrol.* 119: 213-223.

Betts, P.G., Giles, D., Schaefer, B.F., Mark, G. (2007) 1600–1500 Ma hotspot track in eastern Australia: implications for Mesoproterozoic continental reconstructions. *Terra Nova*, 19: 496-501.

Betts, P.G., Giles, D., Foden, F., Schaefer, B.F., Mark, G, Pankhurst, M.J., Caroline Forbes, C.J., Williams, H.A., Chalmers, N.C., Hills, Q. (2009) Mesoproterozoic plume-modified orogenesis in eastern Precambrian Australia, *Tectonics* 28: TC3006, doi:10.1029/2008TC002325.

Buhn, B. (2008) The role of the volatile phase for REE and Y fractionation in low-silica carbonate magmas: implications from natural carbonatites, Namibia. *Mineral. Petrol*. 92: 453 - 470.

Cole, D.R., Drummond, S.E. (1986) Effect of transport and boiling on Ag/Au ratios in hydrothermal solutions: A preliminary assessment and implications for the formation of epithermal precious metal ore deposits.J. Geochem. Explor. 25: 45-79.

Collerson K.D. (2018) Cobalt and HREE mineral systems in the Mount Isa Block. DNRM Report, Dec. 2018, 162pp.

De Andrade, F.R.D., Möller, P., Dulski, P. (2002) Zr/Hf in carbonatites and alkaline rocks: New data and a re-evaluation. *Revista Brasiliera de Geosciências*, 32: 361-370.

Duncan, R.J., Stein, H.J., Evans, K.A., Hitzman, M.W., Nelson, E.P., Kirwin, D.J., (2011) A new geochronological framework for mineralisation and alteration in the Selwyn-Mount Dore corridor, Eastern Fold Belt, Mount Isa Inlier, Australia: Genetic implications for iron oxide copper-gold deposits. *Econ. Geol*., 106: 169-192.

Groves, D.I., Vielreicher, N.M. (2000) The Phalabowra (Palabora) carbonatite-hosted magnetite-copper sulfide deposit, Southe Africa: an end-member of then iron-oxide-copper-gold-rare earth element deposit group? *Mineral. Deposita* 36: 189-194.

Halter, W.E., Pettke, T., & Heinrich CA (2002) The origin of Cu/Au ratios in porphyry-type ore deposits. *Science*, 296: 1844 -1846.

Haynes, D.W., Cross, K.C., Bills, R.T., Reed, M.H., (1995) Olympic Dam ore genesis: A fluid-mixing model: *Econ. Geol.* 90: p. 281–307.

Heinrich. C.A., Günther, D., Audétat, A., Ulrich, T. & Frischknecht, R. (1999) Metal fractionation between magmatic brine and vapor, determined by microanalysis of fluid inclusions. *Geology*, 27: 755–758.

Heinrich, C.A., Halter, W.E., Landtwing, M.R., Pettke, T. (2005) The formation of economic porphyry copper (- gold) deposits: constraints from microanalysis of fluid and melt inclusions. *Geol. Soc. Lond. Spec. Publ.* 248: 247 - 263.

Heinson, G., Didana, Y., Soeffky, P., Thiel, S. & Wise, T. (2018) The crustal geophysical signature of a world-class magmatic mineral system. *Scientific Reports*, 8: 10608.

Johnson, J.P. Cross, K. (1995) U-Pb geochronological constraints on the genesis of the Olympic Dam Cu-U-Au-Ag deposit, South Australia. *Econ. Geol.* 90: 1046–1063.

Kendrick, M.A., Mark, G., Phillips, D. (2007) Mid-crustal fluid mixing in a Proterozoic Fe oxide–Cu–Au deposit, Ernest Henry, Australia: Evidence from Ar, Kr, Xe, Cl, Br, and I. *Earth Planet. Sci. Lett.* 256: 328-343.

Lorand, J-P, Luguet, A. & Alard, O. (2008) Platinum-group elements: A new set of key tracers for the Earth's interior. *Elements*, 4: 247-252.

Loubet, M., Bernat ,M., Javoy, M., Allegre, C.J., (1972) Rare earth contents in carbonatites. *Earth Planet. Sci. Lett.* 14: 226-232.

Marinova, I., Ganev, V., Titorenkova, R. (2013) Colloidal origin of colloform-banded textures in the Paleogene low-sulfidation Khan Krum gold deposit, SE Bulgaria. *Mineral. Deposita*. DOI 10.1007/s00126-013-0473-4.

Marks, L., Keiding, J., Wenzel, T., Trumbull, R.B, Veksler, I., Wiedenbeck, W., Markl, G. (2014) F, Cl, and S concentrations in olivine-hosted melt inclusions from mafic dikes in NW Namibia and implications for the environmental impact of the Paraná–Etendeka Large Igneous Province. *Earth Planet Sci Lett.* 392: 39-49.

McDonough, W. F., Sun S.-S. (1995) The composition of the Earth. *Chem. Geol*., 120: 223–253.

McPhie, J., Kamenetsky, V. S., Allen, S., Ehrig, K. Agangi, A., Bath, A. (2011) The fluorine link between a supergiant ore deposit and a silicic large igneous provinces. *Geology,* 39: 1003-1006.

Mungall, J.E. & Naldrett, A.J. (2008) ore deposits of the platinum-group elements. *Elements*, 4: 253-258.

Oreskes, N., Einaudi, M.T., (1990) Origin of rare earth element-enriched hematite breccias at the Olympic Dam Cu-U-Au-Ag deposit, Roxby Downs, South Australia: *Econ. Geol.*, 85: p. 1–28.

Pokrovski, G.S., Anastassia, Yu., Borisova, A.Y., Harrichoury, J-C. (2008) The effect of sulfur on vapour - liquid fractionation of metals in hydrothermal systems. *Earth Planet. Sci. Lett.* 266:345 -362.

Roberts, D.E., Hudson, G.R.T., (1983) The Olympic Dam copper-uranium- gold deposit, Roxby Downs, South Australia: *Econ. Geol.*, 78: 799–822.

Sillitoe, R.H. (1997) Characteristics and controls of the largest porphyry copper–gold and epithermal gold deposits in the circum-Pacific region. *Aust. J. Earth Sci.* 44: 373–388.

Simon, A.C., Pettke, T., Candela, P.A., Piccoli, P.M., Heinrich, CA (2005) Gold partitioning in melt - vapour - brine systems. *Geochim. Cosmochim. Acta,* 69:3321- 3335.

Simon, AC, Pettke T, Candela PA, Piccoli PM, Heinrich, C.A. (2007) The partitioning behavior of As and Au in S-free and S-bearing magmatic assemblages. *Geochim. Cosmochim. Acta*, 71:1764 - 1782.

Ulrich T, Günther D, Heinrich CA (2001) The evolution of a porphyry Cu–Au deposit, based on LA-ICP-MS analysis of fluid inclusions: Bajo de la Alumbrera, Argentina. *Econ. Geol.* 96:1743–1774.

Wang, L., Duan, J., Simpson J. (2018) Electrical conductivity structures from magnetotelluric data in Cloncurry region. Geoscience Australia Record 2018/05, 47 pp.

Williams, M.R., Holwell, D.A., Lilly, R.M., Case, G.N.D. McDonald, I. (2015) Mineralogical and fluid characteristics of the fluorite-rich Monakoff and E1 Cu–Au deposits, Cloncurry region, Queensland, Australia: Implications for regional F–Ba-rich IOCG mineralisation. Ore Geol. Rev. 64: 103-127.